論文 / 著書情報
Article / Book Information

題目(和文)	原始惑星のまわりの微惑星集団の進化に対するガス抵抗の効果
Title(English)	The Gas Drag Effect on the Evolution of a Planetisimal Swarm around a Protoplanet
著者(和文)	田中秀和
Author(English)	HIDEKAZU TANAKA
出典(和文)	学位:博士(理学), 学位授与機関:東京工業大学, 報告番号:甲第2716号, 授与年月日:1994年3月26日, 学位の種別:課程博士, 審査員:中澤清
Citation(English)	Degree:Doctor of Science, Conferring organization: Tokyo Institute of Technology, Report number:甲第2716号, Conferred date:1994/3/26, Degree Type:Course doctor, Examiner:
学位種別(和文)	博士論文
Type(English)	Doctoral Thesis

The Gas Drag Effect on the Evolution of a Planetesimal Swarm around a Protoplanet

Hidekazu TANAKA

Department of Applied Physics, Tokyo Institute of Technology

February, 1994

(Doctor Thesis)

Abstract

We investigated the long term evolution of the spatial and velocity distribution of a planetesimal swarm around a protoplanet in the late accretion stage, taking account of the effect of gas drag. In the late stage, gravitational scattering by a protoplanet is more effective than that between planetesimals. Hence we neglect scattering between planetesimals and consider the orbital evolution of planetesimals due to scattering by a protoplanet and gas drag by the solar nebula. To describe scattering by a protoplanet, we developed a semi-analytic method of calculating scattering matrices (the changes of the orbital elements) in the three body problem. The derived scattering matrices completely agree with those obtained by numerical orbital integrations in the case of $\frac{1}{3}e < b$ and $(e^2+i^2)^{1/2} \gtrsim 7$. This semi-analytic method accelerates the part of calculating gravitational scattering in our simulation greatly compared to direct orbital integration.

Using the semi-analytic method we simulated orbital evolution of planetesimals around a protoplanet in the nebula gas for $\sim 10^5$ years. We found that scattering by a protoplanet coupled with the gas drag cleans up planetesimals in the feeding zone of the protoplanet as follows. Planetesimals in the vicinity of the protoplanet are scattered strongly. Then the differences in the semimajor axis between the planetesimals and the protoplanet increase as well as the random velocities of the planetesimals. If the gas drag does not exist, the planetesimals are still able to collide with the protoplanet since large random velocities mean large radial excursions. However, the gas drag reduces the enhanced random velocities immediately, which means that planetesimals become impossible to collide with the protoplanet, that is, they go out of the feeding zone of the protoplanet. The timescale of the clean-up is given by $6 \times 10^5 (m/M)^{5/18}$ years. at 1AU, where m and M are the mass of a planetesimal and the protoplanet, respectively.

If the planetesimals in the feeding zone are completely cleaned up, runaway growth of the protoplanet will stop, which causes the problem of formation time of Jovian-type planets again. More refined investigation is needed for planet growth in the solar nebula.

Contents

1 Introduction

It is generally considered that planetary formation proceeded as follows (*e.g.*, Safronov, 1969; Wetherill, 1980; Hayashi *et al.*, 1985). After the formation of disk-like gaseous nebula (which is hereafter called the solar nebula) with mass $\sim 0.02 M_\odot$, where $M_\odot$ is the solar mass, dust grains sink toward the equatorial plane of the solar nebula to form a dust layer. When the density of the dust layer becomes high enough (more exactly, the density becomes as high as the Róche density), the dust layer becomes gravitationally unstable owing to self-gravity force and fragments into a number of small bodies with radius of about 1-10 km, called planetesimals. Afterward, in the gaseous nebula, the planetesimals accumulate to the planets through successive mutual collisions.

The above standard model can roughly explain the present solar system on the basis of physics but has some serious defects. The most serious one is "the formation time problem of the Jovian-type planets", explained below.

Previously it is considered that planetesimals grow through mutual collisions in the following situation: (a) planetesimals grow through colliding with comparable sized bodies ("orderly growth") and (b) their spatial distribution is uniform. Under a uniform spatial distribution of planetesimals, the growth time of planetesimals with mass m, $T_{\mathrm{grow},m} (\equiv m/\dot{m})$, is evaluated as (*e.g.*, Hayashi *et al.*, 1985)

$$T_{\mathrm{grow},m} \simeq \frac{(\frac{4\pi}{3}\rho_{\mathrm{mat}})^{1/3}}{16\pi^2 G \Sigma_{\mathrm{sol}}} v^2 m^{-\frac{1}{3}} \ T_{\mathrm{K}}, \tag{1.1}$$

where Σ_{sol}, ρ_{mat}, and T_{K} are the surface density of solid component in the solar nebula, the material density of planetesimals, and the Keplerian time, respectively, and v is the relative velocity between planetesimals. In the derivation of Eq. (1.1), we assumed that $v \lesssim v_{\mathrm{es}}$ where v_{es} is the escape velocity from the surface of a planetesimal. As seen from the expression (1.1), $T_{\mathrm{grow},m}$ strongly depends on the relative velocity v.

The relative velocity v is approximately given by the random velocity v_{r}, *i.e.*, the

velocity of a deviation from a noninclined circular orbit. The random velocities of planetesimals are excited by mutual gravitational scattering and, on the other hand, dissipated by the drag of the solar nebula gas. Thus, the random velocities is determined by balance between the excitation and the dissipation. Under the assumption (a) (*i.e.*, in a "equal-mass system"), the equilibrium value of the random velocity of planetesimals is given by the escape velocity (*e.g.*, Ohtsuki *et al.*, 1993)

$$v_{\rm r} \simeq v_{{\rm es},m} \equiv \sqrt{\frac{2Gm}{r}} \propto m^{\frac{1}{3}}. \tag{1.2}$$

Substituting the random velocity $v_{\rm r}$ to v in Eq. (1.1), we have the growth time $T_{{\rm grow},m}$ as

$$T_{{\rm grow},m} \sim \begin{cases} 7 \times 10^6 (\frac{m}{10^{28}\ {\rm g}})^{\frac{1}{3}} (\frac{a}{1\ {\rm AU}})^3\ {\rm year}. & {\rm for} \quad a < 2.7\ {\rm AU} \\ \\ 1 \times 10^8 (\frac{m}{10^{28}\ {\rm g}})^{\frac{1}{3}} (\frac{a}{5\ {\rm AU}})^3\ {\rm year}. & {\rm for} \quad a > 2.7\ {\rm AU} \end{cases} \tag{1.3}$$

where we used $\sum_{\rm sol}$ given by Hayashi (1981). In the above, the relation $T_{{\rm grow},m} \propto m^{1/3}$ comes from $v^2 m^{-1/3} \propto m^{1/3}$ and $T_{{\rm grow},m} \propto a^3$ comes from $T_{\rm K}/\sum_{\rm sol} \propto a^{3/2}/a^{-3/2}$. Since the growth time $T_{\rm grow}$ is proportional to $m^{1/3}$, the total formation time of planets is given approximately by the growth time in the last stage of the accretion. Hence, the formation time is evaluated by substituting the solid mass of a present planet into Eq. (1.3). Since $T_{{\rm grow},m} \propto a^3$, the formation time is long for the cores of Jovian-type planets, which is far away from the sun; for Saturn, it is about 1×10^9 years. However, the present Jovian-type planets have massive H/He envelope, which must have been captured from the nebular gas when the core mass becomes about ten times of the Earth mass (Mizuno *et al.*, 1978). Hence their solid cores had to be formed before the dissipation of the nebula gas, *i.e.*, within about $\sim 10^7$ years. This constraint is not satisfied by Eq. (1.3).

Furthermore, Eq. (1.3) shows that the formation time of Neptune is $\sim 2 \times 10^{10}$ years., which is much longer than the solar system age $\sim 4.6 \times 10^9$ years. These are called "the formation time problem of Jovian-type planets"

This problem is supposed to arise from oversimplifications such as assumptions (a) and (b). The recent works (*e.g.*, Wetherill and Stewart, 1989; Ohtsuki and Ida, 1990) have shown that the largest planetesimal (hereafter called "protoplanet") grows more rapidly than the other planetesimals and the mass distribution of planetesimals have a very long high-mass tail: "runaway growth" occurs. Hence, the protoplanet grows through colliding with much smaller bodies than it, that is, the assumption (a) breaks down.

Runaway growth occurs as follows. Due to dynamical friction, the random velocity of the large protoplanet $v_{\mathrm{r},M}$ becomes smaller than that of planetesimals $v_{\mathrm{r},m}$ (Stewart and Wetherill, 1988; Ida, 1990; Ida and Makino, 1992). Then, the relative velocity between a protoplanet and planetesimals is given by the random velocity of planetesimals $v_{\mathrm{r},m}$. We consider the growth times of two protoplanets with masses M_1 and M_2. Since the relative velocity is common, the ratio of the growth times of the protoplanets is (see Eq. (1.1))

$$\frac{T_{\mathrm{grow},M1}}{T_{\mathrm{grow},M2}} = \left(\frac{M_2}{M_1}\right)^{1/3}. \tag{1.4}$$

If the protoplanet M_1 is larger than M_2, $T_{\mathrm{grow},M1}$ become smaller than $T_{\mathrm{grow},M2}$ and *vice versa.* Hence, the large protoplanet grows more rapidly than small one.

Runaway growth shortens the growth time of a protoplanet, since relative velocity v is much smaller in the runaway growth than in the orderly growth as shown below. Since dynamical friction is effective, $v \sim v_{\mathrm{r},m}$. In the early stage of the accretion, the total mass of planetesimals is much larger than the mass of the protoplanet. Hence the random velocity $v_{\mathrm{r},m}$ is regulated by the scattering between planetesimals rather than

by the protoplanet. Then, the random velocity of planetesimals is given by their escape velocity $v_{\mathrm{es},m}$, which is smaller than $v_{\mathrm{es},M}$ (the relative velocity in the orderly growth) by a factor $(m/M)^{1/3}$. On the other hand, in the late stage, the strong gravity of the large protoplanet regulates the random velocity of planetesimals. Even in this stage, $v_{\mathrm{r},m}$ is smaller than $v_{\mathrm{es},M}$. In this case, the protoplanet gravity equilibrates with the gas drag to the planetesimals, while it equilibrates with gas drag to the protoplanet itself in the orderly growth (equal-mass system). Since gas drag is more effective for small bodies, equilibrium velocity is smaller in the runaway growth (non equal-mass system). Through simple estimation, Ida and Makino (1993) gives $v_{\mathrm{r},m} \sim (1/\alpha)v_{\mathrm{es},M}$, where the constant α is several. Also in this case, the growth time of the protoplanet becomes longer as it grows (Ida and Makino, 1993). Hence, the total formation time is given by $T_{\mathrm{grow},M}$ in the last stage. Because of the above effect, the growth time $T_{\mathrm{grow},M}$ becomes smaller than Eq. (1.3) by a factor $(1/\alpha)^2$:

$$T_{\mathrm{grow},M} \simeq (\frac{1}{\alpha})^2 T_{\mathrm{grow},M}(1.3). \tag{1.5}$$

Consequently, the formation time of the cores of Jovian-type planets is fairly shortened, which, at a glance, seems to solve the formation time problem.

However, in the late stage of accretion, the protoplanet makes the spatial distribution of planetesimals non-uniform as shown by Ida and Makino (1993). They studied the evolution of velocity and spatial distribution of a system of one protoplanet and many small planetesimals by direct N-body simulations. They found that when $M/m \gtrsim 100$, the gravitational force of the protoplanet overwhelms the gravitational interaction between planetesimals to make the nonuniformity around the protoplanet (if the latter is more effective, it smoothes out nonuniformity). Hence, the above assumption (b) also breaks down as well as (a). Since a uniform distribution is assumed in its derivation, the growth time (1.5) is not correct for the late accretion stage. We have to know the nonuniform

spatial distribution in order to obtain correct formation time of planets.

Ida and Makino (1993) did not perform the long term calculation and therefore neglected the gas drag force having effect in a long timescale. Thus, it is not clear what the spatial distribution of planetesimals is realized actually.

In the present study, we investigate the long term evolution of the spatial and velocity distribution of planetesimals in the late runaway stage, taking account of the effect of the gas drag; The gas drag does not only decrease the random velocities e and i of planetesimals but also makes them spiral toward the sun gradually to have large effects on the spatial distribution of planetesimals (Adachi *et al.*, 1976). In particular, we will be concerned with the following two questions:

- How does the spatial and velocity distribution of the planetesimals is realized in the vicinity of the protoplanet?

- What effect does the obtained nonuniform distribution have on the planet growth?

We consider the late accretion stage where the scattering by a protoplanet is much more effective than that by planetesimals. Hence, we neglect the interaction between the planetesimals and calculate the orbital evolution of planetesimals due to the effects of the gravity of the protoplanet and the gas drag. The validity of the neglect of interaction between planetesimals is guaranteed for $M/m \gtrsim 100$ by Ida and Makino (1993). Since calculation of all interactions between planetesimals is much hard in numerical calculations, its neglect enables us to perform long term calculations

In the next section, we describe encounters between protoplanet and planetesimal in the solar gravitational field. In Section 3, we introduce a new method of calculating semi-analytically the scattering matrices of high-energy encounters and summarize the scattering matrices we used in our simulation. Since encounters between a protoplanet and a planetesimal in the solar gravitational field is three-body problem, our method is not simple. However, using the semi-analytic method, we can obtain the scattering

matrices much more readily than integrating orbits directly. In Section 4, we explain our model of planetesimal-protoplanet system and method of simulations. We also describe the orbital evolution due to the gas drag. In Section 5, we show the resultant spatial and velocity distributions of a planetesimal swarm around a protoplanet. Our results show that planetesimals go out of the feeding zone of the protoplanet immediately. In the last section, we discuss their effects on the growth of the protoplanet.

2 Two-body Encounters in the Solar Gravitational Field

The random velocities (*i.e.*, eccentricities e^* and inclinations i^*) of planetesimals are enhanced by the mutual gravitational scattering and by the perturbation due to a protoplanet. We consider the latter only, since occasional strong perturbation by a protoplanet is more effective on the increase of the random velocities than successive scattering between planetesimals in the late stage of planet growth we consider.

We will adopt Hill's equation to describe gravitational encounter between a protoplanet and a planetesimal under the solar gravity. Here, we describe Hill's equation only for the present paper. For general properties of Hill's equation., see other articles (*e.g.*, Hénon and Petit, 1986; Nakazawa and Ida, 1988; Nakazawa *et al.*, 1989). We consider a planetesimal with mass m and a protoplanet with mass M. Due to dynamical friction, the eccentricity and inclination of the protoplanet are much smaller than those of the planetesimals (*e.g.*, Stewart and Wetherill, 1989; Ida and Makino, 1992). Hence, we assume that the eccentricity and inclination of the protoplanet are zero (for Hill's equation in the case where the protoplanet has with non-zero eccentricity and inclination, see Nakazawa and Ida, 1988). We adopt the following "Hill's approximations":

$$\begin{cases} m, M \ll M_\odot, \\ e^*, \quad i^* \ll 1, \\ \dfrac{|a - a_0|}{a_0} \ll 1, \end{cases} \tag{2.1}$$

where e^*, i^*, and a are the eccentricity, inclination, and semimajor axis of planetesimal, respectively, and $M_\odot$ and a_0 are the mass of sun and the semimajor axis of the protoplanet.

In the approximation (2.1), for the description of the motion of the planetesimals, it is convenient to use relative coordinates (x, y, z) from the protoplanet, which is called Hill's coordinates, defined by

$$\begin{cases} x = (r^* - a_0)/ha_0, \\ y = (\theta^* - \Omega_0 t)/h, \\ z = z^*/ha_0, \end{cases} \tag{2.2}$$

where (r^*, θ^*, z^*) are the heliocentric cylindrical coordinates, Ω_0 is the Keplerian angular velocity at a_0, and h is the reduced Hill radius defined by

$$h \equiv (\frac{m+M}{3M_\odot})^{1/3}. \tag{2.3}$$

Hill radius ha_0 is the radius within which the gravitational force of the protoplanet is greater than tidal force in the rotating frame. Hereafter, we scale length by ha_0 and time by Ω_0^{-1}.

Since we assume that the protoplanet moves on the noninclined circular orbit of the semimajor axis a_0, it is always sited at $(x, y, z) = (0, 0, 0)$. The motion of the planetesimal is described, in the approximation (2.1), by Hill's equations:

$$\begin{cases} \ddot{x} &= 2\dot{y} &+3x &-\frac{3x}{r^3}, \\ \ddot{y} &= -2\dot{x} & &-\frac{3y}{r^3}, \\ \ddot{z} &= & -z &-\frac{3z}{r^3}, \end{cases} \tag{2.4}$$

where

$$r^2 = x^2 + y^2 + z^2. \tag{2.5}$$

In the above, $2\dot{y}$ and $-2\dot{x}$ are the Coriolis force, $3x$ and $-z$ are the tidal force, and the last terms proportional to r^{-3} represent the gravitational force of the protoplanet.

We have a Keplerian motion as a solution of Eq. (2.4) when the mutual gravity can be neglected:

$$\begin{cases} x = b - e\cos(t-\tau), \\ y = \lambda - \dfrac{3}{2}bt + 2e\sin(t-\tau), \\ z = i\sin(t-\omega), \end{cases} \tag{2.6}$$

and

$$\begin{cases} v_x = e\sin(t-\tau), \\ v_y = -\dfrac{3}{2}b + 2e\cos(t-\tau), \\ v_z = i\cos(t-\omega). \end{cases} \tag{2.7}$$

Here the constants $(\lambda, b, e, \tau, i, \omega)$ correspond to the Keplerian orbital elements. The orbital element b is defined by

$$b = \frac{a - a_0}{ha_0}, \tag{2.8}$$

and e and i are the reduced eccentricity and inclination defined by

$$\begin{cases} e = e^*/h, \\ i = i^*/h. \end{cases} \tag{2.9}$$

The phase angles λ, τ and ω are related to the time of perihelion passage, the argument of perihelion and the longitude of ascending node. When the planetesimal approach the protoplanet these values are not constant owing to the gravitational interaction. Consequently, these elements after the encounter are different from those of before the encounter.

Substituting Eqs. (2.6) and (2.7) into Hill's equation (2.4) and $\boldsymbol{v} = \dot{\boldsymbol{x}}$, we have equations describing the evolution of the orbital elements $(b, \lambda, e, \tau, i, \omega)$ as (Hasegawa and Nakazawa, 1990)

$$\begin{cases} \dot{b} = 2F_y, \\ \dot{\lambda} = -2F_x + 3tF_y, \\ \dot{e}^2 = 2v_xF_x + 4(3x + 2v_y)F_y, \\ e^2\dot{\tau} = -(3x + 2v_y)F_x + 2v_xF_y, \\ \dot{i}^2 = 2v_zF_z, \\ i^2\dot{\omega} = zF_z, \end{cases} \tag{2.10}$$

where $\boldsymbol{F} \equiv -3\boldsymbol{r}/r^3$ is the gravitational force of the protoplanet.

It should be noted that e, i, and b cannot change independently. In Hill's equation (2.4), as is well known, there exists an energy integral called the Jacobi integral, which is given by (*e.g.*, Nakazawa *et al.*, 1989)

$$E_{\mathrm{J}} = \frac{1}{2}(e^2 + i^2) - \frac{3}{8}b^2 - \frac{3}{r} + \frac{9}{2}. \tag{2.11}$$

From the conservation of E_{J}, if e and i increase through encounter, b have to increase.

3 Scattering Matrices in Two-body Encounters

It is not generally possible to solve Hill's equation analytically, because it is the three-body problem. In some cases, however, we can obtain the orbital change due to an encounter analytically or by simple numerical calculations. For distant encounters with $b \gtrsim e, i, 1$ or horseshoe orbits with very small b, scattering matrices (the changes of orbital elements) have been obtained analytically by Hasegawa and Nakazawa (1990) (referred to as HN90).

We newly developed a semi-analytic method of calculating scattering matrices for close encounters. The derived scattering matrices completely agree with those obtained by numerical orbital integrations in the case of high-energy encounters, $(e^2 + i^2)^{1/2} \gtrsim 7$. Using the method we have developed, we can obtain changes of orbital elements much more immediately than integrating orbits directly.

3.1. The plan of the calculation

We calculate the changes of the orbital elements, Δb, Δe^2, and Δi^2, as functions of incident orbital elements $(b_0, \lambda_0, e_0, \tau_0, i_0, \omega_0)$. For the other orbital elements, we can also calculate their changes in a similar way but do not here because we do not need them in our simulations as will be seen later. Note that without loss of generality we can put $\lambda_0 = 0$ in our calculation. Such a special choice of λ_0 corresponds to that we redefine the phases τ_0 and ω_0 of epicycle motion and vertical oscillation as those at the synodic moments. Thus initial conditions of orbits are specified by five elements $(b_0, e_0, \tau_0, i_0, \omega_0)$.

As shown in Eq. (2.10), Δb, Δe^2, and Δi^2 are obtained by integrating the gravitational force of the protoplanet $\boldsymbol{F}$. To calculate $\boldsymbol{F}$, we have to specify the orbits of planetesimals. As seen below, we can obtain the orbits in a good accuracy when $e^2 + i^2 \gg 1$. Hence, hereafter, we are concentrated on high-energy encounters with $e^2 + i^2 \gg 1$. First, we determine the approximate orbit around the closest approach, because the orbital elements mainly change around the closest point $\boldsymbol{r}_{\rm min}$. Then we calculate the gravitational

force $\boldsymbol{F}$ along the orbit. Second, substituting obtained $\boldsymbol{x}$, $\boldsymbol{v}$, and $\boldsymbol{F}$ into Eq. (2.10) and integrating it during a encounter, we calculate the change of orbital elements Δb, Δe^2, and Δi^2.

3.2. Determination of orbits around the closest approach

To determine the orbits around the closest approach, first we find the closest point $\boldsymbol{r}_{\rm min}$ and the velocity at the point $\boldsymbol{v}_{\rm min}$ from Eqs. (2.6) and (2.7), assuming that orbits are nearly unperturbed Keplerian until the closest approach. Next, we consider the orbit near the closest point accurately.

From Hill's equations (2.4), the magnitude of forces acting planetesimals near the closest point are evaluated as

$$\begin{cases} \text{the Coriolis force} & \sim & v_{\rm min}, \\ \text{the tidal force} & \sim & r_{\rm min}, \\ \text{the mutual gravitational force} & \sim & \dfrac{3}{r_{\rm min}^2}, \end{cases} \tag{3.1}$$

where $v_{\rm min} = |\boldsymbol{v}_{\rm min}|$ and $r_{\rm min} = |\boldsymbol{r}_{\rm min}|$. Let $\Delta v_{\rm Cori}$, $\Delta v_{\rm tid}$, $\Delta v_{\rm 2B}$ be the changes of the velocity due to the Coriolis force, the tidal force, and the gravity of the protoplanet, respectively. Multiplying those forces by the approximate scattering period $\Delta t \sim r_{\rm min}/v_{\rm min}$, we evaluate the changes of the velocity as

$$\begin{cases} \Delta v_{\rm Cori}/v_{\rm min} \sim r_{\rm min}/v_{\rm min}, \\ \Delta v_{\rm tid}/v_{\rm min} \sim (r_{\rm min}/v_{\rm min})^2, \\ \Delta v_{2B}/v_{\rm min} \sim \dfrac{3}{r_{\rm min} v_{\rm min}^2}. \end{cases} \tag{3.2}$$

Thus, when $r_{\rm min} \ll v_{\rm min}$, the Coriolis force and the tidal force can be neglected during the scattering, while the mutual gravity is negligible during the scattering when $r_{\rm min} \gg$

$3/v_{\rm min}^2$. All of the three forces can be regarded to be small perturbations when $\alpha \cdot 3/v_{\rm min}^2 < r_{\rm min} < v_{\rm min}/\beta$, where α and β are some constants larger than unity.

Empirically, taking $\alpha = 2$ and $\beta = 3$, we divide the encounters into the following three cases: (1) $r_{\rm min} \leq 6/v_{\rm min}^2$, (2) $r_{\rm min} \geq v_{\rm min}/3$, and (3) $6/v_{\rm min}^2 < r_{\rm min} < v_{\rm min}/3$. Figure 1 shows Δb obtained by direct orbital integration (eighth order Runge-Kutta method) for $e_0 = 10, i_0 = 0$, and $b_0 = 5$. In this case Δb is a function of only τ_0. In this figure Regimes 1, 2, and 3, determined as the above criterion are shown; Regime 1 corresponds to strong scattering region ($r_{\rm min} \leq 6/v_{\rm min}^2$), Regime 2 corresponds to weak scattering region ($r_{\rm min} \geq v_{\rm min}/3$), and Regime 3 is intermediate region ($6/v_{\rm min}^2 < r_{\rm min} < v_{\rm min}/3$). For each regime, the approximate orbit around the closest approach is obtained in the following way.

Regime 1: $r_{\rm min} \leq 6/v_{\rm min}^2$.

In this case, as seen from Eq. (3.2), the changes of the velocity $\Delta v_{\rm Cori}$ and $\Delta v_{\rm tid}$ is very small in the high-energy encounters ($v_{\rm min} \gg 1$) because $\Delta v_{\rm Cori}/v_{\rm min} \lesssim 6/v_{\rm min}^3$ and $\Delta v_{\rm tide}/v_{\rm min} \lesssim (6/v_{\rm min}^3)^2$. Thus, the approximate orbit around the closest approach is obtained by Hill's equations (2.10) with neglecting the Coriolis force and the tidal force in them. Then, the solution is no more than two-body Keplerian orbit around the protoplanet, $\boldsymbol{r}_{\rm 2B}$, which can be obtained analytically.

Regime 2: $r_{\rm min} \geq v_{\rm min}/3$

In this regime, the gravity of the protoplanet is negligible because $\Delta v_{\rm 2B}/v_{\rm min} \lesssim 9/v_{\rm min}^3 \ll 1$. Thus, the approximate orbit is the Keplerian orbit around the sun given by Eqs. (2.6) and (2.7).

Regime 3: $6/v_{\rm min}^2 < r_{\rm min} < \frac{v_{\rm min}}{3}$

In this case, all the three changes of the velocity are small: $\Delta v_{\rm Cori}/v_{\rm min} < 1/3$, $\Delta v_{\rm tid}/v_{\rm min} < 1/9$, and $\Delta v_{2B}/v_{\rm min} < 1/2$. Thus, during the scattering, the orbit is roughly given by a straight line, $\boldsymbol{r}_{\rm st} \equiv \boldsymbol{r}_{\rm min} + \boldsymbol{v}_{\rm min}(t - t_{\rm min})$, where $t_{\rm min}$ is the

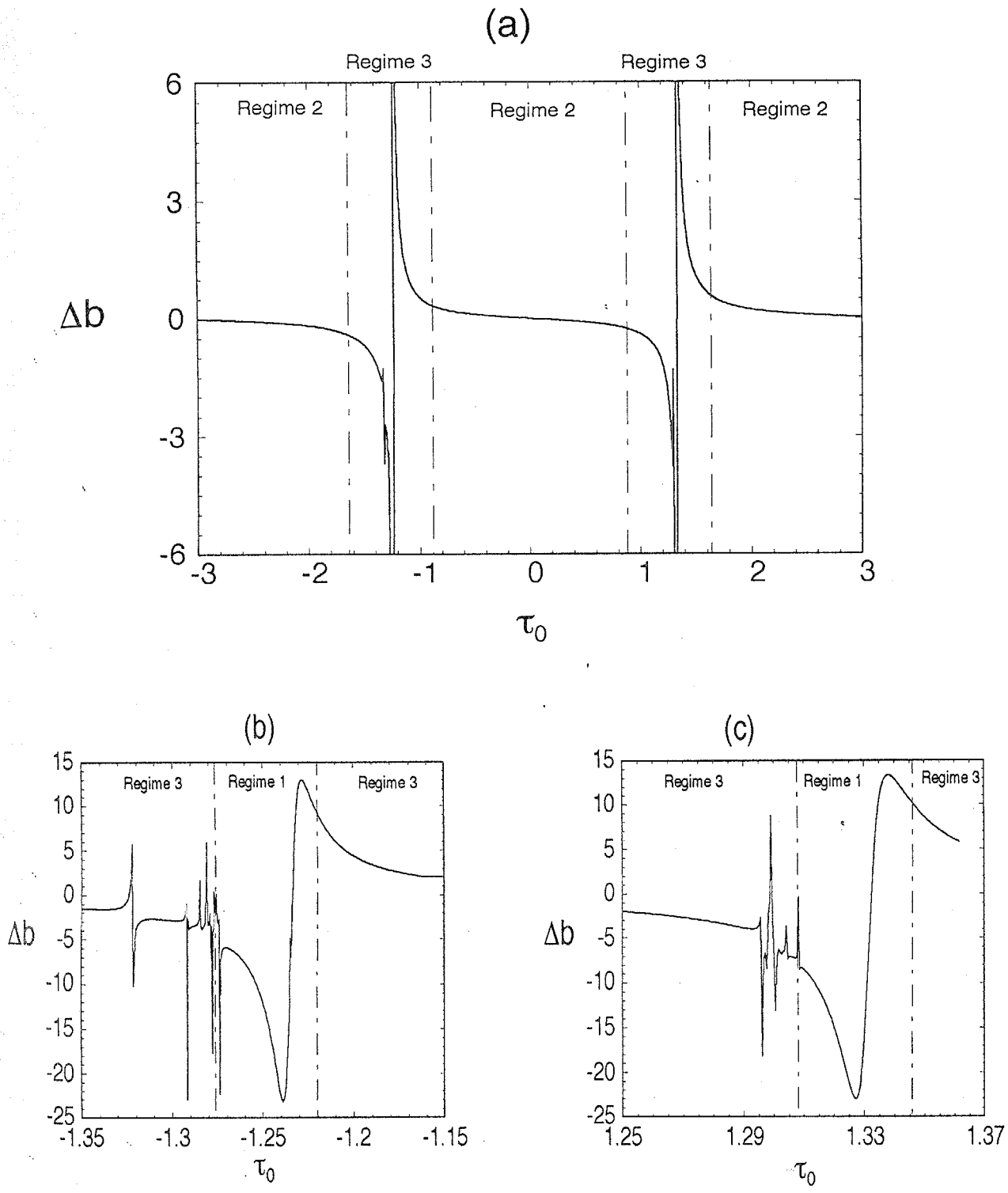

Fig. 1. The change of the orbital element Δb calculated by numerical integration of orbits in the case of $e_0 = 10$ and $b_0 = 5$. Ranges of Regime 1,2, and 3 are shown. Figure 1(b) and (c) are magnifications of Fig. 1(a) at $\tau_0 = -1.3$ (a) and 1.3 (b).

time at the closest point. However, the changes of the velocity are not sufficiently small. Hence, in order to obtain the approximate orbit as we need, we further take account of the effect of the three forces as perturbations.

In the above, we assumed that $v_{\min}$ is sufficiently large. The velocity $v_{\min}$ is approximately equal to $(e_0^2 + i_0^2 - \frac{3}{4}b_0^2)^{1/2}$ (see Eq. (A.9)). Hence, the above approximations are correct when $e_0^2 + i_0^2 - \frac{3}{4}b_0^2 \gg 1$.

3.3. Calculation of the scattering matrices in the high-energy encounters

(i) Regime 1: $r_{\min} \leq 6/v_{\min}^2$.

Since the Coriolis force and the tidal force are negligible in this case, Hill's equation (2.4) is reduced to that of the two-body Keplerian motion:

$$\dot{\boldsymbol{v}} = \boldsymbol{F}(\equiv -\frac{3\boldsymbol{r}}{r^3}). \tag{3.3}$$

In the same approximation, we put $x = 0$ on the right hand side in Eqs. (2.10). Then, with Eq. (3.3), Eqs. (2.10) read

$$\begin{cases} \dot{b} = 2\dot{v}_y, \\ \dot{e}^2 = 2v_x\dot{v}_x + 8v_y\dot{v}_y, \\ \dot{i}^2 = 2v_z\dot{v}_z. \end{cases} \tag{3.4}$$

Equations (3.4) can be readily integrated and, as a result, we have the changes of orbital elements as

$$\begin{cases} \Delta b & \equiv \int \dot{b}dt & = 2\Delta v_y, \\ \Delta(e^2) & \equiv \int \dot{e}^2 dt & = \Delta(v_x)^2 + 4\Delta(v_y)^2, \\ \Delta(i^2) & \equiv \int \dot{i}dt & = \Delta(v_z)^2, \end{cases} \tag{3.5}$$

where Δv_i and $\Delta(v_i)^2$ are the changes of v_i and v_i^2 due to a scattering. The formula (3.5) was also obtained by Ida *et al.* (1993). In order to obtain the scattering matrices, we only have to know the velocity $\boldsymbol{v}$ before and after scattering.

To know them, we need the incident velocity $\boldsymbol{v}_i$ for two-body scattering and the two-body impact parameter ρ between the planetesimal and the protoplanet. In this case, $\boldsymbol{v}_i$ and ρ are given by $\boldsymbol{v}_{\rm min}$ and $r_{\rm min}$, respectively. The closest point $\boldsymbol{r}_{\rm min}$ and the velocity $\boldsymbol{v}_{\rm min}$ at the point of the Keplerian orbit Eqs. (2.6) and (2.7) are obtained in a complicated way as shown in Appendix. Here, we calculate the scattering matrices, assuming that $\boldsymbol{r}_{\rm min}$ and $\boldsymbol{v}_{\rm min}$ have been obtained.

The orbit of the planetesimal is on the plane spanned by the vectors $\boldsymbol{r}_{\rm min}$ and $\boldsymbol{v}_{\rm min}$. The scattering angle $\Delta\theta$ is given by a well-known formula (*e.g.*, Landau and Lifshitz 1957):

$$\Delta\theta = 2\sin^{-1}\left(\frac{1}{\sqrt{A^2+1}}\right) \tag{3.6}$$

with

$$A = \frac{r_{\rm min} v_{\rm min}^2}{3}. \tag{3.7}$$

Using $\boldsymbol{r}_{\rm min}$, $\boldsymbol{v}_{\rm min}$ and $\Delta\theta$, we have the velocity after scattering $\boldsymbol{v}_{\rm final}$ as

$$\begin{aligned}\boldsymbol{v}_{\rm final} &= v_{\rm min}\cos(\Delta\theta)\hat{\boldsymbol{v}}_{\rm min} - v_{\rm min}(\sin\Delta)\theta\hat{\boldsymbol{r}}_{\rm min} \\ &= \boldsymbol{v}_{\rm min} - \frac{2v_{\rm min}}{A^2+1}(\hat{\boldsymbol{v}}_{\rm min} + A\hat{\boldsymbol{r}}_{\rm min}),\end{aligned} \tag{3.8}$$

where $\hat{\boldsymbol{r}}_{\rm min} = \boldsymbol{r}_{\rm min}/r_{\rm min}$ and $\hat{\boldsymbol{v}}_{\rm min} = \boldsymbol{v}_{\rm min}/v_{\rm min}$.

Substituting Eq. (3.8) into the right hand side in Eq. (3.5), we finally obtain

$$
\begin{cases}
\Delta b = & -\dfrac{4}{A^2+1}(v_{\min,y} + A\dfrac{v_{\min}}{r_{\min}} r_{\min,y}), \\
\Delta e^2 = & -\dfrac{4}{A^2+1}[v_{\min,x}^2 + 4v_{\min,y}^2 + A\dfrac{v_{\min}}{r_{\min}}(v_{\min,x} r_{\min,y} + 4v_{\min,y} r_{\min,y})] \\
& -\dfrac{4}{(A^2+1)^2}(v_{\min,x} + A\dfrac{v_{\min}}{r_{\min}} r_{\min,x})^2 \\
& -\dfrac{16}{(A^2+1)^2}(v_{\min,y} + A\dfrac{v_{\min}}{r_{\min}} r_{\min,y})^2, \\
\Delta i^2 = & -\dfrac{4}{A^2+1}(v_{\min,z} + A\dfrac{v_{\min}}{r_{\min}} v_{\min,z} r_{\min,y}) \\
& -\dfrac{4}{(A^2+1)^2}(v_{\min,z} + A\dfrac{v_{\min}}{r_{\min}} r_{\min,z})^2,
\end{cases}
\tag{3.9}
$$

where $r_{\min,i}$ and $v_{\min,i}$ are i-components ($i = x, y, z$) of $\boldsymbol{r}_{\min}$ and $\boldsymbol{v}_{\min}$, respectively. In Figs. 2(a) and 2(b), Δb given by Eq. (3.9) is compared with that obtained by direct orbital integration. They are deviated from each other in the direction of τ_0. As seen from Figs. 2(c) and 2(d),however, they are in complete agreement with each other (except for narrow chaotic zones) by adequate shifts of τ_0. Although our semi-analytic method does not seem to be adequate to describe individual orbits exactly, the above shift of τ_0 makes no problem for our study since our aim is to clarify the statistical behavior of a planetesimal swarm. In chaotic zones around $\tau_0 = -1.31$ and 1.23, the semi-analytic method fails to reproduce the numerical result. In these zones, planetesimals encounter two or more times, which is not taken account of in our semi-analytic method. However, the fractional volume of the chaotic zone in phase space is sufficiently small and, then, we can neglect this difference. We found a quite similar feature also in comparing Δe^2.

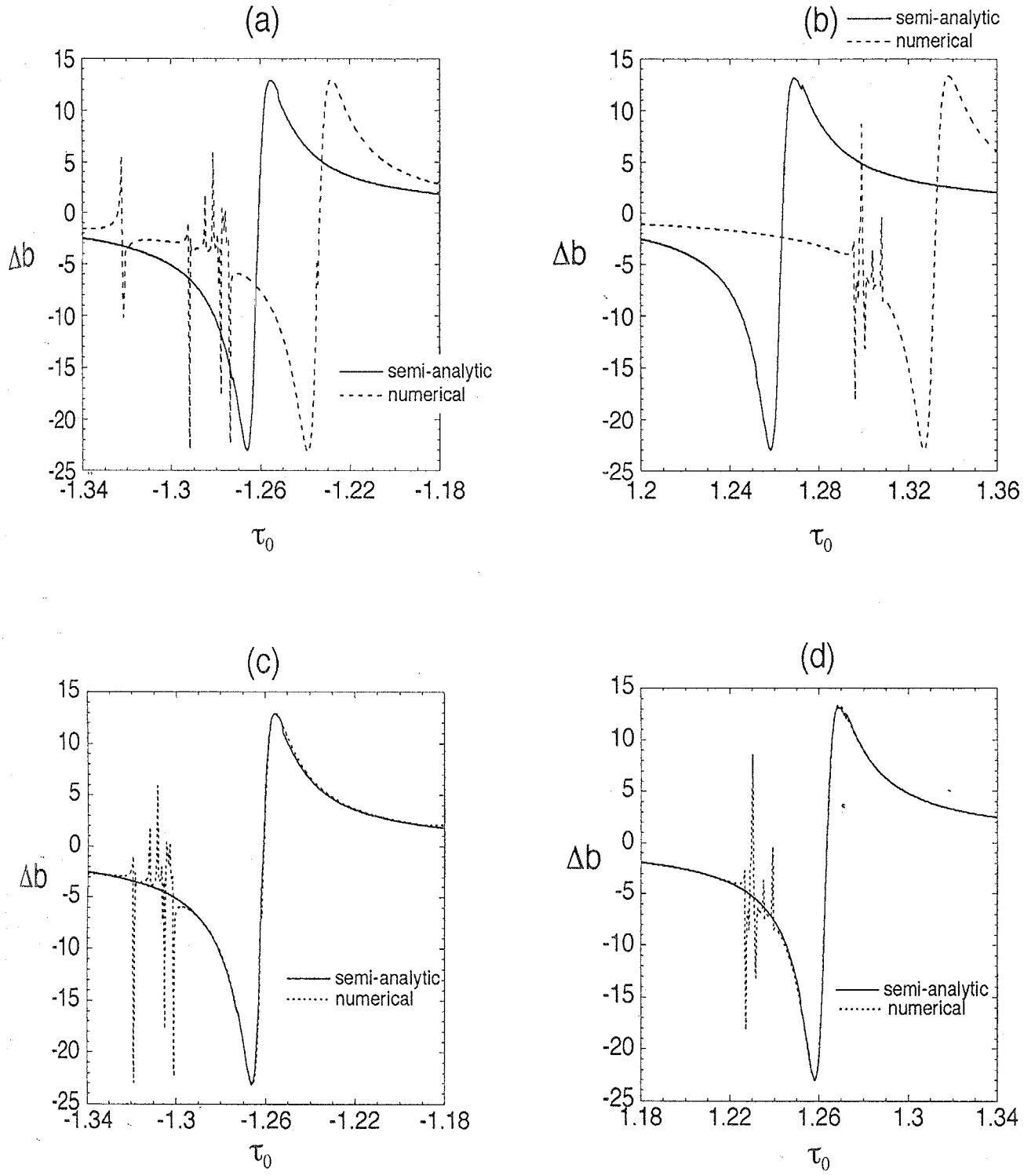

Fig. 2. The change Δb obtained by our semi-analytic method in the case of $e_0 = 10$ and $b_0 = 5$ (denoted by the solid curve) for Regime 1. The numerical result in the same case (denoted by the dotted line) is compared. They agree well with each other, if τ_0 is suitably shifted.

(ii) Regime 2: $r_{\rm min} \geq v_{\rm min}/3$

In this case, the approximate orbit is the heliocentric Keplerian orbit $\boldsymbol{r}_{\rm sun}$ (2.6). Integrating the right hand side of Eq. (2.10) along $\boldsymbol{r}_{\rm sun}$, we can obtain the scattering matrices. It is impossible to perform this integration analytically. Hence, we integrated them numerically (with the trapezoidal rule). To integrate them in a good accuracy, it is sufficient to take timesteps as ~ 0.2, which is much larger than that required in direct orbital integration; hence, our method to obtain $\Delta b, \Delta e^2$, and Δi^2 is much faster than direct orbital integration. Figure 3 shows that Δb thus obtained is in good agreement with that obtained by direct orbital integration in this regime, too.

(iii) Regime 3: $6/v_{\rm min}^2 \leq r_{\rm min} \leq v_{\rm min}/3$

In this case, the Coriolis force, the tidal force, and the mutual gravity are all small. The approximate orbit around the closest approach is roughly given by the straight line $\boldsymbol{r}_{\rm st}$ which is tangent to the Keplerian orbit $\boldsymbol{r}_{\rm sun}$ at its closest point $\boldsymbol{r}_{\rm min}$. However, in this case, all forces are not small enough to be neglected completely. Hence, we obtain the more accurate orbit around the closest approach, taking $\boldsymbol{r}_{\rm st}$ as an unperturbed orbit and all forces as small perturbations. The deviation of the orbit due to the mutual gravity $\delta\boldsymbol{r}_{\rm 2B}$ is given by

$$\delta\boldsymbol{r}_{\rm 2B} = \boldsymbol{r}_{\rm 2B} - \boldsymbol{r}_{\rm st}. \tag{3.10}$$

And the deviation due to the Coriolis force and the tidal force $\delta\boldsymbol{r}_{\rm sun}$ is

$$\delta\boldsymbol{r}_{\rm sun} = \boldsymbol{r}_{\rm sun} - \boldsymbol{r}_{\rm st}. \tag{3.11}$$

Hence, the approximate orbit $\boldsymbol{r}_{\rm app}$ is expressed as

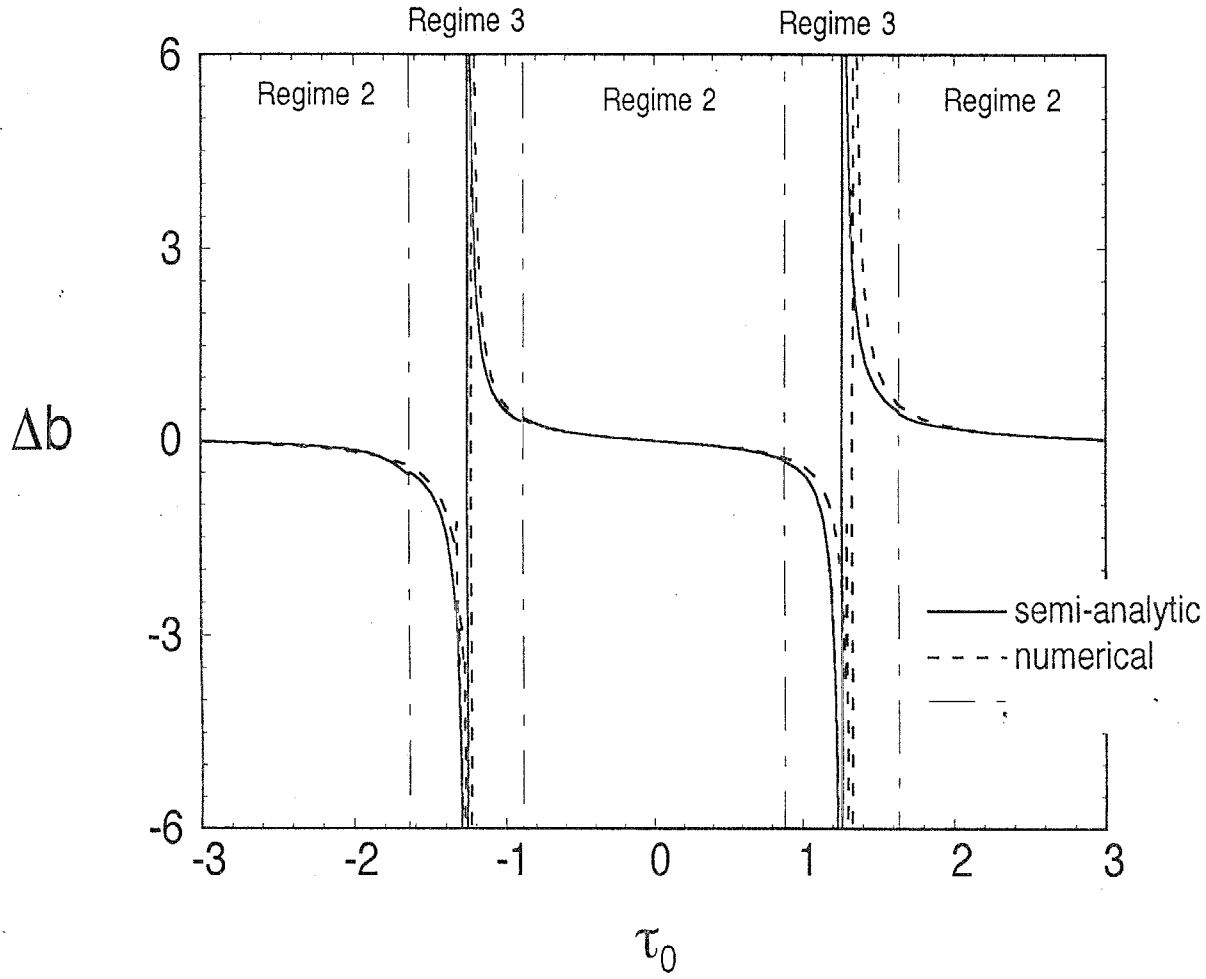

Fig. 3. The semi-analytic result is compared with the numerical result for Regime 2 and 3.

$$\begin{aligned} \boldsymbol{r}_{\rm app} &= \boldsymbol{r}_{\rm st} + \delta\boldsymbol{r}_{\rm 2B} + \delta\boldsymbol{r}_{\rm sun} \\ &= \boldsymbol{r}_{\rm sun} + \boldsymbol{r}_{\rm 2B} - \boldsymbol{r}_{\rm st}. \end{aligned} \tag{3.12}$$

In the above expression, we neglected the coupling terms due to the Coriolis force and the gravity, because they are $O(\frac{3}{v_{\rm min}^3} \cdot r_{\rm min})$ $(\ll |\boldsymbol{r}_{\rm min}|)$.

In a similar way as $\boldsymbol{r}_{\rm app}$, we can obtain Δb, Δe^2, and $\Delta^2 i$. For example, we show the way of calculating Δb. The change Δb is expressed as

$$\begin{aligned} \Delta b &= \Delta b(\boldsymbol{r}_{\rm st}) + [\Delta b(\boldsymbol{r}_{\rm 2B}) - \Delta b(\boldsymbol{r}_{\rm st})] + [\Delta b(\boldsymbol{r}_{\rm sun}) - \Delta b(\boldsymbol{r}_{\rm st})] \\ &= \Delta b(\boldsymbol{r}_{\rm sun}) + \Delta b(\boldsymbol{r}_{\rm 2B}) - \Delta b(\boldsymbol{r}_{\rm st}), \end{aligned} \tag{3.13}$$

where $\Delta b(\boldsymbol{r}_i)$ (i = sun, 2B, and st) is the change of b obtained when the orbit $\boldsymbol{r}_i$ is substituted into Eq. (2.10). We have already obtained $\Delta b(\boldsymbol{r}_{\rm 2B})$ in Eq. (3.9). The change $\Delta b(\boldsymbol{r}_{\rm st})$ can be readily obtained as follows. Since $\boldsymbol{r}_{\rm st}$ is unperturbed orbit, $\boldsymbol{r}_{\rm st}$ does not include a small parameter $1/A$ $(\equiv 3/(r_{\rm min} v_{\rm min}^2))$ which is related to the gravity of the protoplanet. On the other hand, because the change Δb is essentially due to the gravity of the protoplanet, $\Delta b(\boldsymbol{r}_{\rm st})$ consists of the terms proportional to $1/A$. Since $\Delta b(\boldsymbol{r}_{\rm st})$ coincides with $\Delta b(\boldsymbol{r}_{\rm 2B})$ up to the first order term of $1/A$, from Eq. (3.9) we have $\Delta b(\boldsymbol{r}_{\rm st})$ as

$$\Delta b(\boldsymbol{r}_{\rm st}) = -4\frac{v_{\rm min}}{r_{\rm min}} r_{{\rm min},y} \frac{1}{A}. \tag{3.14}$$

Hence, the difference $\Delta b(\boldsymbol{r}_{\rm 2B}) - \Delta b(\boldsymbol{r}_{\rm st})$ is given by

$$\Delta b(\boldsymbol{r}_{\rm 2B}) - \Delta b(\boldsymbol{r}_{\rm st}) = -\frac{4}{A^2+1}(v_{{\rm min},y} - \frac{1}{A}\frac{v_{\rm min}}{r_{\rm min}} r_{{\rm min},y}). \tag{3.15}$$

In order to obtain $\Delta b(\boldsymbol{r}_{\rm sun})$, numerical integrations are necessary. We divided the integration range into two parts: the distant part ($|\boldsymbol{r}| \gtrsim v_{\rm min}/2$) and the close part ($|\boldsymbol{r}| \lesssim v_{\rm min}/2$). For the distant part, we integrated Eq. (2.10) numerically as well as calculation in Regime 2. On the other hand, for the close part, we integrated it analytically as follows. Around the closet point $\boldsymbol{r}_{\rm min}$, in an accuracy of the order $r_{\rm min}/v_{\rm min}$, the orbit $\boldsymbol{r}_{\rm sun}$ is given by

$$\begin{aligned}\boldsymbol{r}_{\rm sun} &= \boldsymbol{r}_{\rm min} - \boldsymbol{v}_{\rm min}(t - t_{\rm min}) + \frac{1}{2}\boldsymbol{a}_{\rm min}(t - t_{\rm min})^2 \\ &= \boldsymbol{r}_{\rm st}(t) + \frac{1}{2}\boldsymbol{a}_{\rm min}(t - t_{\rm min})^2, \end{aligned} \tag{3.16}$$

where $t_{\rm min}$ is the time at the closest point and $\boldsymbol{a}_{\rm min} \equiv (\ddot{\boldsymbol{r}}_{\rm sun})_{\rm min}$ is given by (see Eqs. (2.6) and (2.7))

$$\begin{cases} a_{{\rm min},x} &= e\cos(t_{\rm min} - \tau), \\ a_{{\rm min},y} &= -2e\sin(t_{\rm min} - \tau), \\ a_{{\rm min},z} &= -i\sin(t_{\rm min} - \omega). \end{cases} \tag{3.17}$$

In Eq. (3.16), the term $\frac{1}{2}\boldsymbol{a}_{\rm min}(t - t_{\rm min})^2$ is always smaller than $\boldsymbol{r}_{\rm st}$ if $|t - t_{\rm min}| \ll 1$ and, then, higher terms of $|t - t_{\rm min}|$ can be neglected. Hence, we define the close part by $t_{\rm min} - \Delta t \le t \le t_{\rm min} + \Delta t$ with $\Delta t = 0.4$.

In this first order approximation, the gravity of the protoplanet on the orbit $\boldsymbol{r}_{\rm sun}$ is obtained as

$$\begin{aligned}\boldsymbol{F}(\boldsymbol{r}_{\rm sun}) &\equiv -\frac{3\boldsymbol{r}_{\rm sun}}{r_{\rm sun}^3} \\ &= -\frac{3\boldsymbol{r}_{\rm st}(s)}{r_{\rm st}(s)^3} - \frac{3}{2}\boldsymbol{a}_{\rm min}\frac{s^2}{r_{\rm st}(s)^3} + \frac{9}{2}(\boldsymbol{a}_{\rm min}\cdot\boldsymbol{r}_{\rm st}(s))\frac{s^2\boldsymbol{r}_{\rm st}(s)}{r_{\rm st}(s)^5}, \end{aligned} \tag{3.18}$$

where $s = t - t_{\rm min}$. Substituting Eq. (3.18) to Eq. (2.10), we have the change of b in the close part $\Delta b(\boldsymbol{r}_{\rm sun})_{\rm close}$ as

$$\Delta b(\boldsymbol{r}_{\rm sun})_{\rm close} \equiv \int_{-\Delta t}^{\Delta t} 2F_y(\boldsymbol{r}_{\rm sun})ds$$

$$= -12\hat{r}_{{\rm min},y}\frac{\Delta}{r_{\rm min}\sqrt{(v_{\rm min}\Delta t)^2 + r_{\rm min}^2}}$$

$$+ \frac{6}{v_{\rm min}^3}[3(\boldsymbol{a}_{\rm min}\cdot\hat{\boldsymbol{v}}_{\rm min})\hat{v}_{{\rm min},y} - a_{{\rm min},y}] \tag{3.19}$$

$$\times [\ln|\frac{v_{\rm min}\Delta t + \sqrt{(v_{\rm min}\Delta t)^2 + r_{\rm min}^2}}{r_{\rm min}}| - \frac{v_{\rm min}\Delta t}{\sqrt{(v_{\rm min}\Delta t)^2 + r_{\rm min}^2}}]$$

$$+ \frac{6}{v_{\rm min}^3}[(\boldsymbol{a}_{\rm min}\cdot\hat{\boldsymbol{r}}_{\rm min})\hat{r}_{{\rm min},y} - (\boldsymbol{a}_{\rm min}\cdot\hat{\boldsymbol{v}}_{\rm min})\hat{v}_{{\rm min},y}]\frac{(v_{\rm min}\Delta t)^3}{((v_{\rm min}\Delta t)^2 + r_{\rm min}^2)^{3/2}},$$

where $\hat{\boldsymbol{r}}_{\rm min} = \boldsymbol{r}_{\rm min}/r_{\rm min}$ and $\hat{\boldsymbol{v}}_{\rm min} = \boldsymbol{v}_{\rm min}/v_{\rm min}$. This expression is correct in an accuracy of the order $r_{\rm min}/v_{\rm min}$, In our method, we adopt an expression in the second order approximation, which is obtained in a similar way.

In this way, we obtained Δb (3.13). Figure 3 shows that Δb thus obtained is in good agreement with that obtained by direct orbital integration except for slight shift of τ_0. This shift makes no problem for our simulation as mentioned before. The changes of other orbital elements, Δe^2 and Δi^2 are obtained in a similar way.

3.4. Limits of the semi-analytical method

We showed that our semi-analytical method completely reproduces scattering matrices in the case of $e_0 = 10, i_0 = 0$, and $b_0 = 5$. Next we have to make clear what ranges of (e_0, i_0, b_0) our method is applicable for.

First we examine the range of b_0. We found that for the case of $b_0 \lesssim e_0/3$, our semi-analytic method is inapplicable. In Fig. 4, the case of $e_0 = 10$ and $b_0 = 3.5$ is shown as an example. The semi-analytic result (Fig. 4(a)) qualitatively differs from the numerical

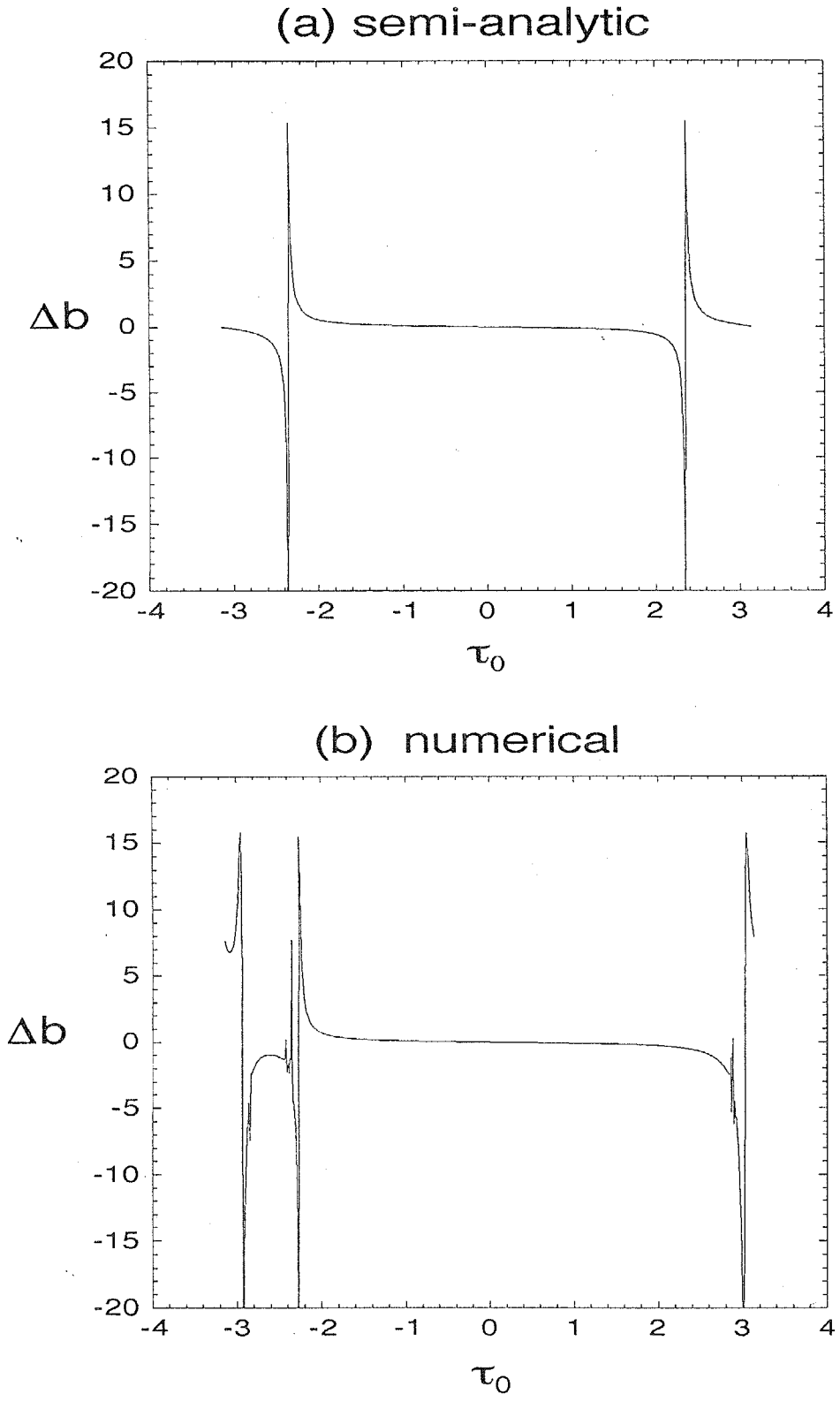

Fig. 4. Comparison between the semi-analytic result (a) and the result of numerical orbital integration (b) in the case of $e_0 = 10$ and $b_0 = 3.5$. In the result of orbital integration, three peaks exist. One of them ($\tau_0 \simeq -3$) does not appear in the semi-analytic result.

one (Fig. 4(b)), especially about $\tau_0 \simeq -3$. This difference is due to the occurrence of the two-times encounter, which is not taken into account in our method. Generally, when $b_0 \lesssim e_0/3$, the two-times encounter frequently occurs and, thus, it cannot be ignored.

We also found that our method does not make accurate results at $b_0 \simeq e_0$, but this discrepancy can be recovered by shifting b_0 slightly, as shown below. In Fig. 5, we showed the case where $e_0 = 10$ and $b_0 = 10$. The semi-analytic result almost agree with the numerical one when $|\Delta b|$ is small (see Fig. 5(a)). On the other hand, when $\tau \simeq 0$, as seen from Fig. 5(b), the two results qualitatively differ from each other. In Fig. 5(c), the semi-analytic result for the case of $e_0 = 10$, $b_0 = 9.9$ is compared with the result of numerical orbital integration for the case of $e_0 = 10$, $b_0 = 10$. These two results agree well with each other. Such a shift of Δb in the direction of b_0 is not important in our simulation. Thus, the semi-analytic method is valid for the case where $e_0 \simeq b_0$, too. For $b_0 > e_0$, the semi-analytic method gives correct results.

Next we examine the ranges of e_0 and i_0. The semi-analytic method is invalid when neither the incident e_0 nor i_0 are large enough. Since the incident velocity $v_{\rm min}$ roughly given by $(e_0^2 + i_0^2)^{1/2}$, the assumption $v_{\rm min} \gg 1$ is not satisfied then. Actually, as seen from Fig. 6, the two results do not agree well with each other for the "low-energy" case where $e_0 = 5, i_0 = 0$, and $b_0 = 2.5$. We found that our method is not applicable for $(e_0^2 + i_0^2)^{1/2} \lesssim 7$.

Finally, we also show a three dimensional case (*i.e.*, $i_0 \neq 0$). In Fig. 7, the case of $e_0 = 10$, $b_0 = 5$ and $i_0 = 5$ is presented. We compared the semi-analytic result for the phase angle $\omega_0 = 2.308$ with the numerical one for $\omega_0 = 2.375$, shifting τ_0. The two results agree well with each other. As mentioned above, the slight shifts of phase angles τ_0 and ω_0 are not important. Thus, the semi-analytic method is also valid for three dimensional cases.

After all, our semi-analytic method is applicable in the condition that (i)$b_0 \gtrsim e_0/3$, (ii)$(e_0^2 + i_0^2)^{1/2} \gtrsim 7$.

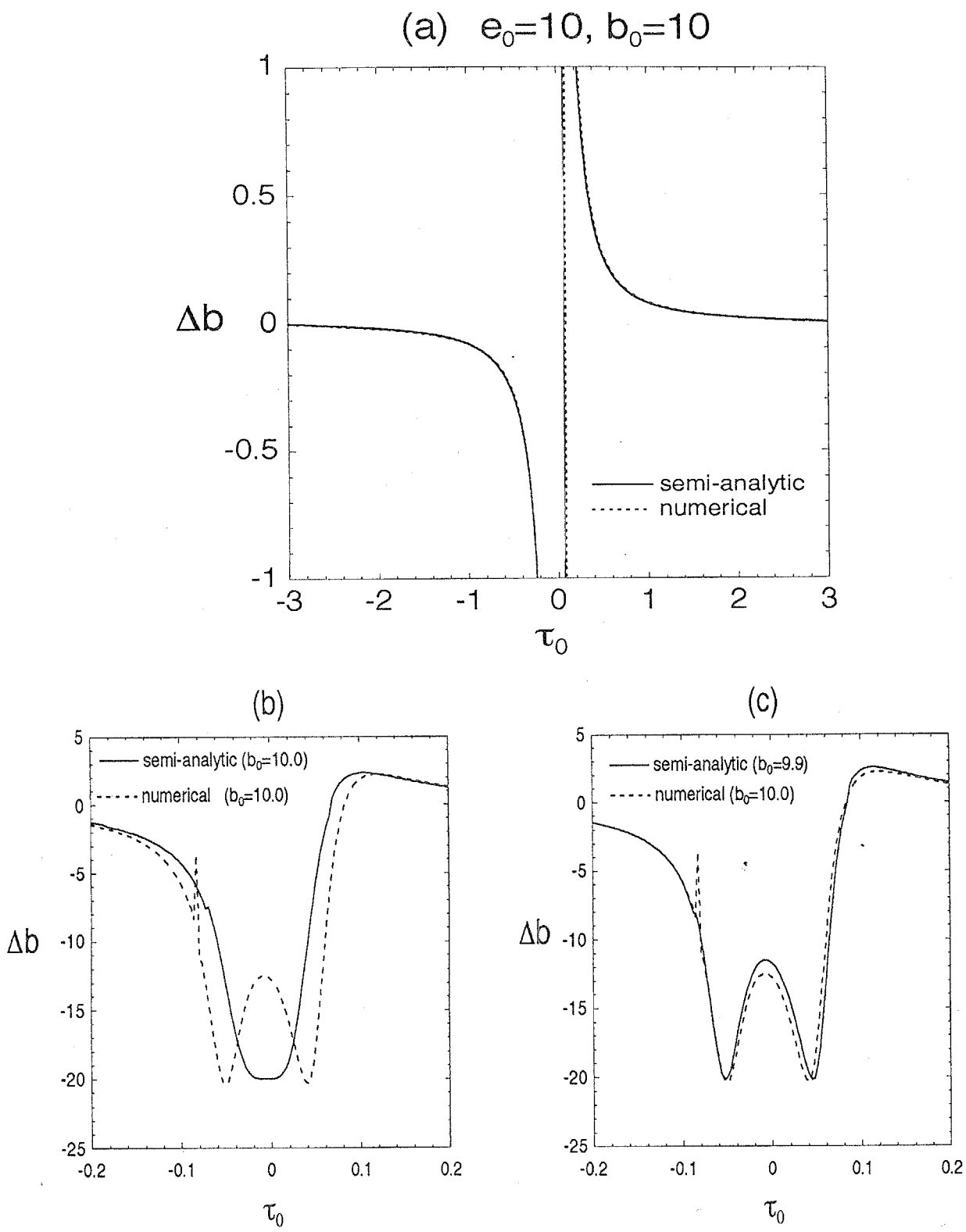

Fig. 5. In Panels (a) and (b), we made a comparison for the case of $e_0 = 10$, $b_0 = 10$. As seen from Panel (b), the semi-analytic result fairly differs from the exact value near $\tau_0 \simeq 0$. In Panel (c), the semi-analytic result for $e_0 = 10$ and $b_0 = 9.9$ is compared with the numerical one for $e_0 = 10$ and $b_0 = 10$. These two curves agree well with each other.

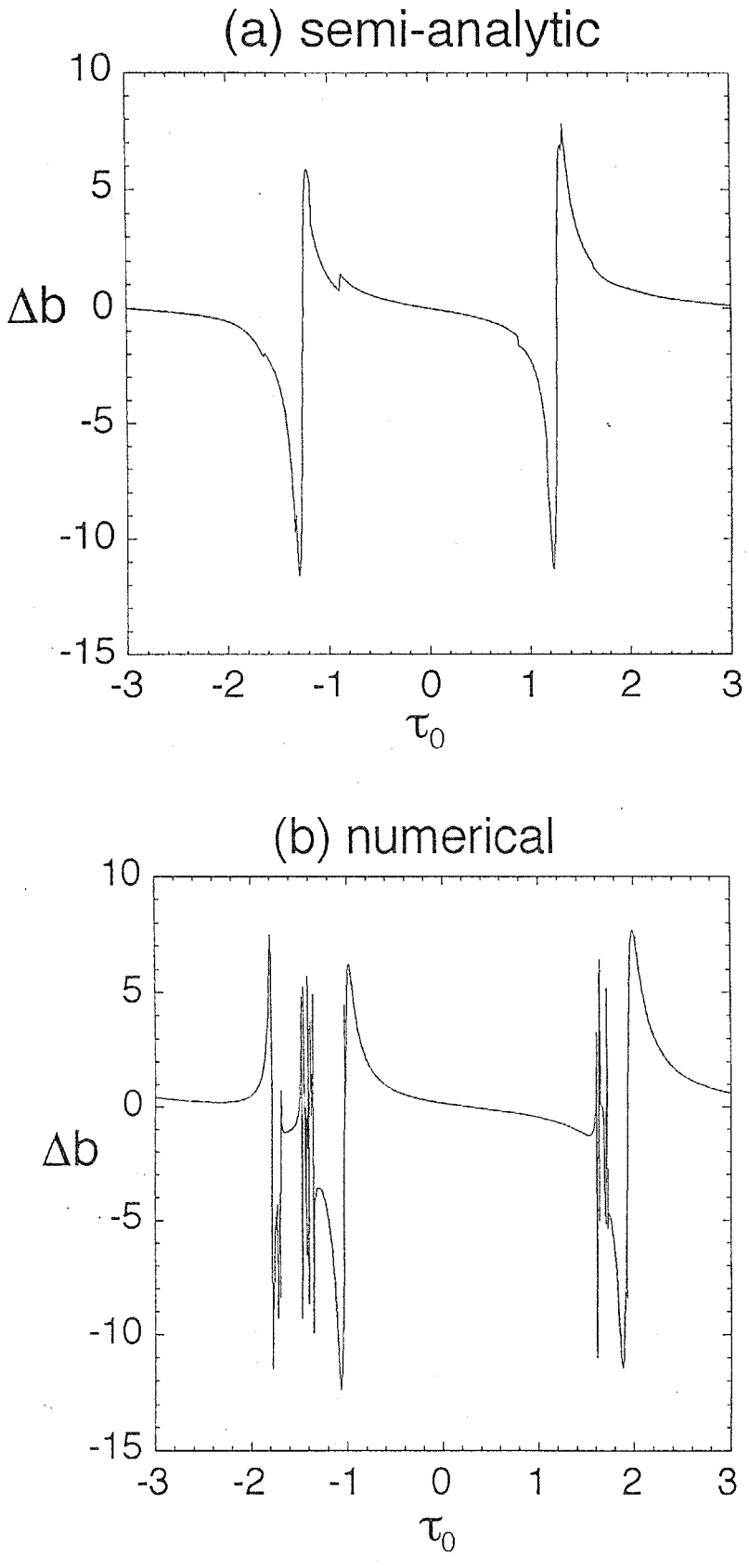

Fig. 6. Comparison in the "low-energy" case of $e_0 = 5$ and $b_0 = 2.5$. The semi-analytic result (a) considerably differs from the numerical one (b) in the range where Δb become large.

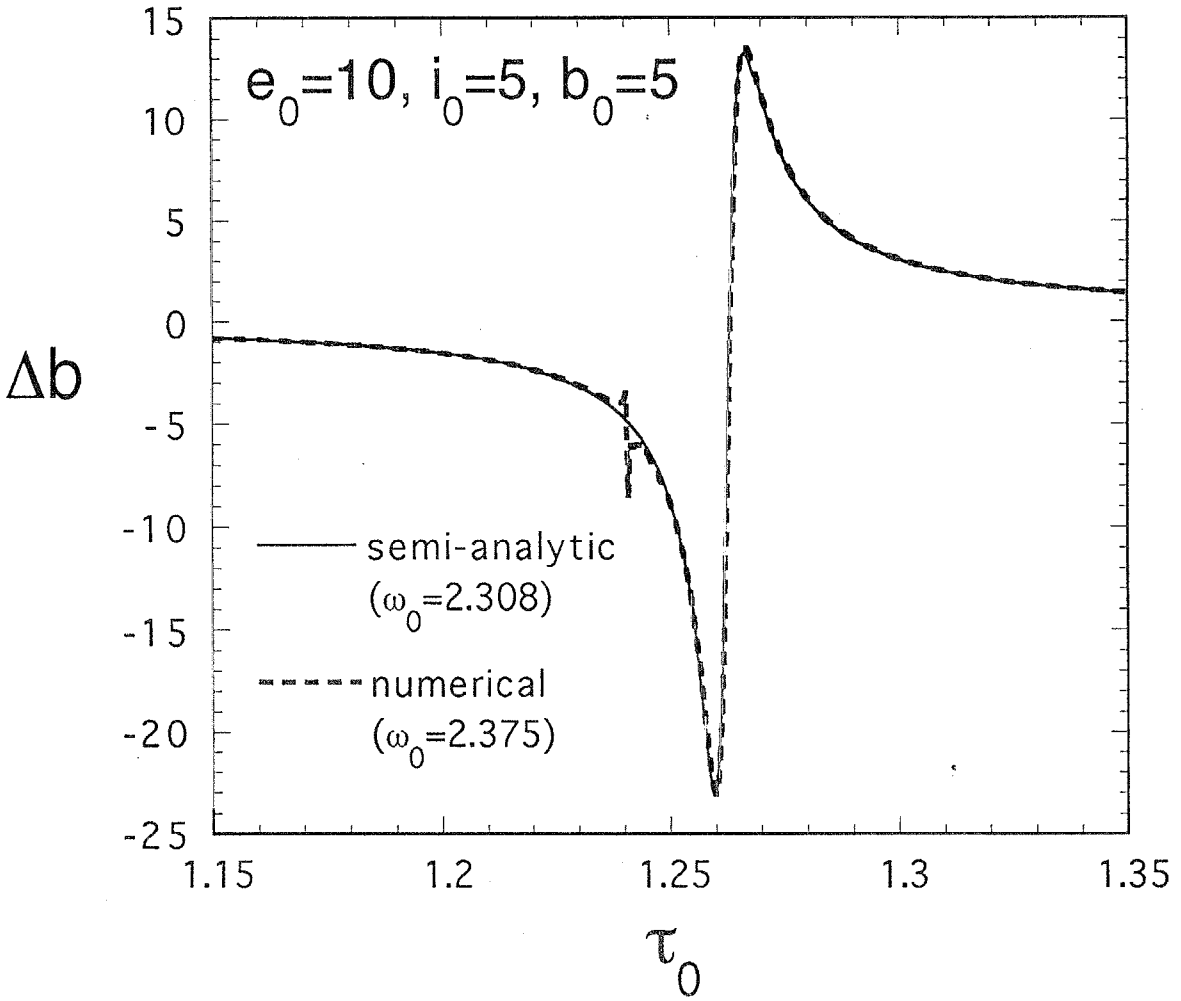

Fig. 7. Comparison in the three dimensional case (where $e_0 = 10$, $b_0 = 5$, and $i_0 = 5$). By slight shifts of τ_0 and ω_0, we can fit the semi-analytic result on the numerical one.

3.5. Distant encounters

Analytic expressions of the scattering matrices have been known in two special cases (HN90): b_0 is (1) very small or (2) large enough. The latter case is covered by the semi-analytic method, but procedure to obtain scattering matrices by HN90 is much simpler than that by the semi-analytic method. Hence, we use the result by HN90 for the latter case. Since the former case cannot be covered by the semi-analytic method, we of course use the result by HN90 for the former case. Here we summarize the results by HN90.

In the former case, an orbit is so called "horseshoe orbit". In this case the scattering matrices Δb, Δe^2, and Δi^2 are approximately given by

$$\begin{cases} \Delta b = -2b_0, \\ \Delta e^2 = \Delta i^2 = 0. \end{cases} \tag{3.20}$$

This approximation is correct when the following inequality is satisfied:

$$\frac{8}{b_0^2} - 2e_0 \gg 1. \tag{3.21}$$

Hence, we adopt Eq.(3.20) when $8/b_0^2 - 2e_0 > 8$, *i.e.*,

$$|b_0| < \sqrt{\frac{4}{e_0 + 4}}. \tag{3.22}$$

In the later case ("distant encounter"), the changes Δe^2 and Δi^2 are approximately given by

$$\begin{cases} \Delta e^2 = & \frac{18}{b_0^2}[R_1 p_2 + R_2 \frac{p_1 p_2}{b_0} + (R_4 - R_6)\frac{p_1^2 p_2}{b_0^2} - R_7 \frac{p_2^3}{b_0^2} \\ & + R_5 \frac{p_1 q_1 q_2}{b_0^2} - R_8 \frac{q_1^2 p_2}{b_0^2} - R_9 \frac{q_2^2 p_2}{b_0^2}] + \frac{81 R_1^2}{b_0^4}, \\ \Delta i^2 = & \frac{18}{b_0^3}[R_3 q_1 q_2 + (R_{10} + R_{11})\frac{p_1 q_1 q_2}{b_0} + (R_5 \frac{p_2 q_1^2}{b_0^2} \\ & - R_5 \frac{p_2 q_2^2}{b_0^2}], \end{cases} \tag{3.23}$$

where $(p_1, p_2) \equiv (e_0 \cos\tau_0, e_0 \sin\tau_0)$ and $(q_1, q_2) \equiv (i_0 \cos\omega_0, i_0 \sin\omega_0)$. In the above, R_1 to R_{11} are constants consisting of modified Bessel functions, which is approximately given by

$$\begin{cases} R_1 = 0.747, \quad R_2 = 2.38, \quad R_3 = 0.210, \quad R_4 = 3.46, \\ R_5 = 0.147, \quad R_6 = -1.86, \quad R_7 = 1.73, \quad R_8 = 0.149, \\ R_9 = 0.476, \quad R_{10} = 0.766, \quad R_{11} = -0.379. \end{cases} \tag{3.24}$$

Furthermore, using the above Δe^2 and Δi^2, Δb is given by

$$\Delta b = \frac{2}{3b_0}[\Delta e^2 + \Delta i^2]. \tag{3.25}$$

These expressions are correct when $b_0 \gg e_0, i_0, 1$. Hence, we use Eqs. (3.23) and (3.25) if the inequality

$$|b_0| > \max(2e_0, 1.7i_0, e_0 + 3) \tag{3.26}$$

is satisfied.

3.6. Summary of scattering matrices

We summarize how to get $\Delta b, \Delta e^2$, and Δi^2 in our calculation.

(i) $|b_0| < \sqrt{\dfrac{4}{e_0+4}}$:
use Eq. (3.20).

(ii) $|b_0| > \max(2e_0, 1.7i_0, e_0+3)$:
use Eqs. (3.23) and (3.25).

(iii) $\max(2e_0, 1.7i_0, e_0+3) < |b_0| < \sqrt{\dfrac{4}{e_0+4}}$

(a) $(e_0^2+i_0^2)^{1/2} \geq 7$:

use the semi-analytic method stated in Section 3.3.

(b) $(e_0^2+i_0^2)^{1/2} < 7$:

perform direct orbital integration by forth order Runge-Kutta method.

We use the semi-analytic method also in the case of $b_0 \leq e_0/3$ where it is invalid. The encounters in which $b_0 \leq e_0/3$ occur less frequently than others since number of planetesimals encountering with the protoplanet per unit time is proportional to b_0 (shear velocity is proportional to b_0). Hence, if we use the semi-analytic method also in such a case, it may affect the results of simulations little.

For the case of (iiib), we must perform direct orbital integration. However, the orbital integration in this low-velocity case is easier than that in the high-velocity case. In the high-velocity case, orbital elements change only due to close encounters. Hence it is necessary to obtain accurate scattering matrices in high-velocity close encounters. To do this by orbital integrations, we must take very short timesteps, which make the computation time long. On the other hand, in the low-velocity case, close encounters are not important because orbital elements mainly change in non-close encounters which occur much more frequently than close encounters. Consequently, using our semi-analytic method for high-velocity case, we can considerably reduce the computation time in our simulation.

4 Modeling of Planetesimal-Protoplanet System

We calculate the orbital evolution of an equal-mass planetesimal swarm in the vicinity of a protoplanet. Generally, the orbits of planetesimals changes due to the three effects: the gravitational force by the protoplanet, mutual gravitational interactions between planetesimals, and the drag force by the solar nebula gas. As mentioned before, we neglect the second effect since we investigate late accretion stage. Hence, in our calculation, we consider the gravity of the protoplanet and the gas drag force.

Due to Keplerian shear, planetesimals encounter the protoplanet every synodic period $T_{\rm s}$. At each encounter with the protoplanet the orbital elements of planetesimals are changed by the gravitational perturbation of the protoplanet. The gas drag force changes their orbital elements continuously. Since the timescale of a gravitational scattering is comparable to the Keplerian period $T_{\rm K}$, it is much shorter than the synodic period $T_{\rm s}$ (see Eq. (4.1)). Thus, the gas drag force changes the orbits mainly during intervals between encounters when the planetesimals do not interact with the protoplanet; during the scattering by the protoplanet, the gas drag force can be neglected.

Hence we can divide the process of the orbital evolution of planetesimals into the two steps:

1. the impulsive orbital change due to scattering by the protoplanet.

2. the gradual orbital evolution due to the gas drag force during intervals between the scatterings.

These two steps are repeated by turns and, as a result, the evolution of the spatial and velocity distribution of planetesimals is obtained.

We consider the evolution of distribution of the orbital elements e, i, and b which express the magnitude of random velocity and the radial position. On the other hand, we are not concerned with phase angles, assuming that they are randomly distributed.

(a) Scattering by the protoplanet

Planetesimals encounter the protoplanet every synodic period T_s due to Keplerian shear motion. As seen in Eq. (2.7), the shear velocity between a planetesimal and a protoplanet is given by $\frac{3}{2}|b|hv_K$, where v_K is Keplerian velocity. The synodic period T_s is the time taken to go around by the shear velocity, which is given by

$$\begin{aligned} T_s &= \frac{2\pi a}{\frac{3}{2}|b|hv_K} \\ &= \frac{2}{3|b|h}T_K. \end{aligned} \tag{4.1}$$

In the above, we used $T_K = 2\pi a/v_K$. The changes of Δb, Δe^2, and Δi^2 can be calculated by the method described in Section 3 if initial conditions $(b_0, e_0, i_0, \tau_0, \omega_0)$ are specified. The initial values b_0, e_0, and i_0 are given by the resultant values in the last encounter added by the changes due to the gas drag after the last encounter. Initial values of τ_0 and ω_0 are given by random number, assuming they are randomly distributed in $[0, 2\pi]$.

(b) Gas drag

The orbital evolution due to the gas drag force was investigated by Adachi *et al.* (1976). They derived the change rates of orbital elements as

$$\begin{cases} \dfrac{de}{dt} = -\dfrac{e}{T_0}\left(\dfrac{5}{8}e^2 + \dfrac{1}{2}i^2 + (\eta/h)^2\right)^{1/2}, \\ \dfrac{di}{dt} = -\dfrac{i}{2T_0}\left(\dfrac{5}{8}e^2 + \dfrac{1}{2}i^2 + (\eta/h)^2\right)^{1/2}, \\ \dfrac{db}{dt} = -\dfrac{2\eta/h}{T_0}\left(\dfrac{5}{8}e^2 + \dfrac{1}{2}i^2 + (\eta/h)^2\right)^{1/2}, \end{cases} \tag{4.2}$$

where T_0 is the characteristic timescale of the gas drag and η is the (fractional) deviation of the gas velocity v_g from Keplerian velocity $v_{\rm K}$ due to the pressure gradient defined by

$$\eta = \frac{v_{\rm K} - v_{\rm g}}{v_{\rm K}}. \tag{4.3}$$

The characteristic time T_0 is defined by

$$T_0 = \frac{2m}{C_{\rm D}\pi r^2 \rho_{\rm gas}(hv_{\rm K})}, \tag{4.4}$$

where $C_{\rm D}$ is the gas drag coefficient (~ 1) and $\rho_{\rm gas}$ is the density of the solar nebula gas. That is, T_0 is the dissipation time for the case where relative velocity between a planetesimal and gas is unit velocity $hv_{\rm K}$. In the low mass solar nebula model (Hayashi, 1981), T_0 and η are given explicitly as

$$\begin{cases} T_0 = \dfrac{2.6 \times 10^3}{hC_{\rm D}} \left(\dfrac{m}{10^{24}{\rm g}}\right)^{\frac{1}{3}} \left(\dfrac{a}{1{\rm AU}}\right)^{\frac{7}{4}} T_{\rm K}, \\ \\ \eta = 2 \times 10^{-3} \left(\dfrac{a}{1{\rm AU}}\right)^{\frac{1}{2}}. \end{cases} \tag{4.5}$$

Equations (4.2) show that the gas drag inhibits the increase of random velocity e, i, and decreases b (*i.e.*, shortens semimajor axis a). Integrating Eq. (4.2) over the time interval between the scattering, $T_{\rm s}$, yields the changes of e, i, and b during the interval.

Since the synodic period $T_{\rm s}$ is usually much smaller than T_0, Eq. (4.2) can be solved iteratively. In an accuracy of the order $(T_{\rm s}/T_0)^2$ we obtain

$$\begin{cases} \Delta e = -e_0 \left[u_0 \left(\dfrac{T_{\rm s}}{T_0}\right) - \dfrac{1+s_0}{2} u_0^2 \left(\dfrac{T_{\rm s}}{T_0}\right)^2 \right], \\ \\ \Delta i = -i_0 \left[u_0 \left(\dfrac{T_{\rm s}}{T_0}\right) - \dfrac{1+2s_0}{8} u_0^2 \left(\dfrac{T_{\rm s}}{T_0}\right)^2 \right], \\ \\ \Delta b = -\dfrac{2\eta}{h} \left[u_0 \left(\dfrac{T_{\rm s}}{T_0}\right) - \dfrac{s_0 u_0^2}{2} \left(\dfrac{T_{\rm s}}{T_0}\right)^2 \right], \end{cases} \tag{4.6}$$

where e_0 and i_0 are the initial values of e and i and the functions u_0 and s_0 are defined by

$$\begin{cases} u_0 = [\frac{5}{8}e_0^2 + \frac{1}{2}i_0^2 + (\eta/h)^2]^{\frac{1}{2}}, \\ \\ s_0 = \dfrac{5e_0^2 + 2i_0^2}{8u_0^2}. \end{cases} \tag{4.7}$$

Since b changes a little during the interval between encounters due to the gas drag, the synodic period T_s deviates slightly from $2T_K/(3|b_0|h)$. In Eq. (4.6), we use a more accurate expression of T_s:

$$T_s = \frac{2T_K}{3|b_0|h}[1 + \frac{2\eta u_0 b_0}{3h^2|b_0|^2 T_0}]. \tag{4.8}$$

In our simulation, we adopt Eq. (4.6) as changes Δe, Δi, and Δb due to the gas drag during a interval between scatterings.

(c) Orbit of the protoplanet

Finally, we mention the orbit of the protoplanet. Due to the dynamical friction by the planetesimal swarm, the eccentricity and the inclination of the protoplanet become much smaller than those of planetesimals. Thus we put the eccentricity and the inclination of the protoplanet to zero. The semimajor axis a_M of the protoplanet changes due to the gas drag and reaction to scattering a large number of planetesimals. In our model, we take account of both effects, but the latter is more important as follows. Since $T_0 \propto m^{1/3}$, the characteristic timescale of the gas drag for the protoplanet $T_{0,M}$ is larger than that for planetesimals (denoted by T_0 hereafter) by a factor $(M/m)^{1/3}$. That is, the migration speed of a planetesimal swarm is faster than that of the protoplanet. As will

be shown in the next section, the reaction of encounters works so that the migration of the protoplanet coincides with that of a planetesimal swarm and, hence, the protoplanet migrates with timescale T_0 rather than with $T_{0,M}$ (except for the last stage when the mass of the protoplanet is as large as the total mass of planetesimals).

5 Results

5.1. The gas drag effect on the planetesimal-protoplanet system

According to the model described in Section 4, we simulated the long term evolution of planetesimals around a protoplanet in nebula gas. To see how the gas drag influences orbital evolutions of planetesimals, we first compare the result in the nebula gas with that in the gas-free case.

(i) The gas-free case

We performed the simulation of 700 planetesimals with $m = 1 \times 10^{24}$g and a protoplanet with $M = 5 \times 10^{25}$g on the following initial conditions:

1. The semi-major axis of the protoplanet a_M is 1AU.

2. The distributions of e and i of planetesimals are Gaussian with the dispersions $\langle e^2 \rangle^{1/2} = 2\langle i^2 \rangle^{1/2} = 2$.

3. The planetesimals are uniformly distributed in the range of $-\dot{2}0 < b < 20$ [*i.e.*, $(1-20h)\mathrm{AU} < a < (1+20h)\mathrm{AU}$] to satisfy that the surface mass density Σ equals 7 $\mathrm{g\,cm^{-2}}$, which is consistent with the low mass ($\sim 0.02 M_\odot$) solar nebula model. The region is taken to be so large that the radial width is sufficiently larger than the mean radial excursion ($\sim ea$) of planetesimals.

In Fig. 8, we plot the spatial and velocity distributions of planetesimals at time (a) $t = 0$, (b) 1×10^4, and (c) 5×10^4 years. In these figures, ordinates $(e^2 + i^2)^{1/2}$ express the magnitude of the random velocity and abscissas b express the radial position relative to the protoplanet. The protoplanet is at the origin (*i.e.*, $b = 0$ and $e = i = 0$). As seen from Fig. 8(b) and (c), due to the gravitational perturbation of the protoplanet, the planetesimals in the vicinity of the protoplanet are pushed aside and their random velocities increase. In Fig. 8, we also plotted the contours of Jacobi energy E_J when a

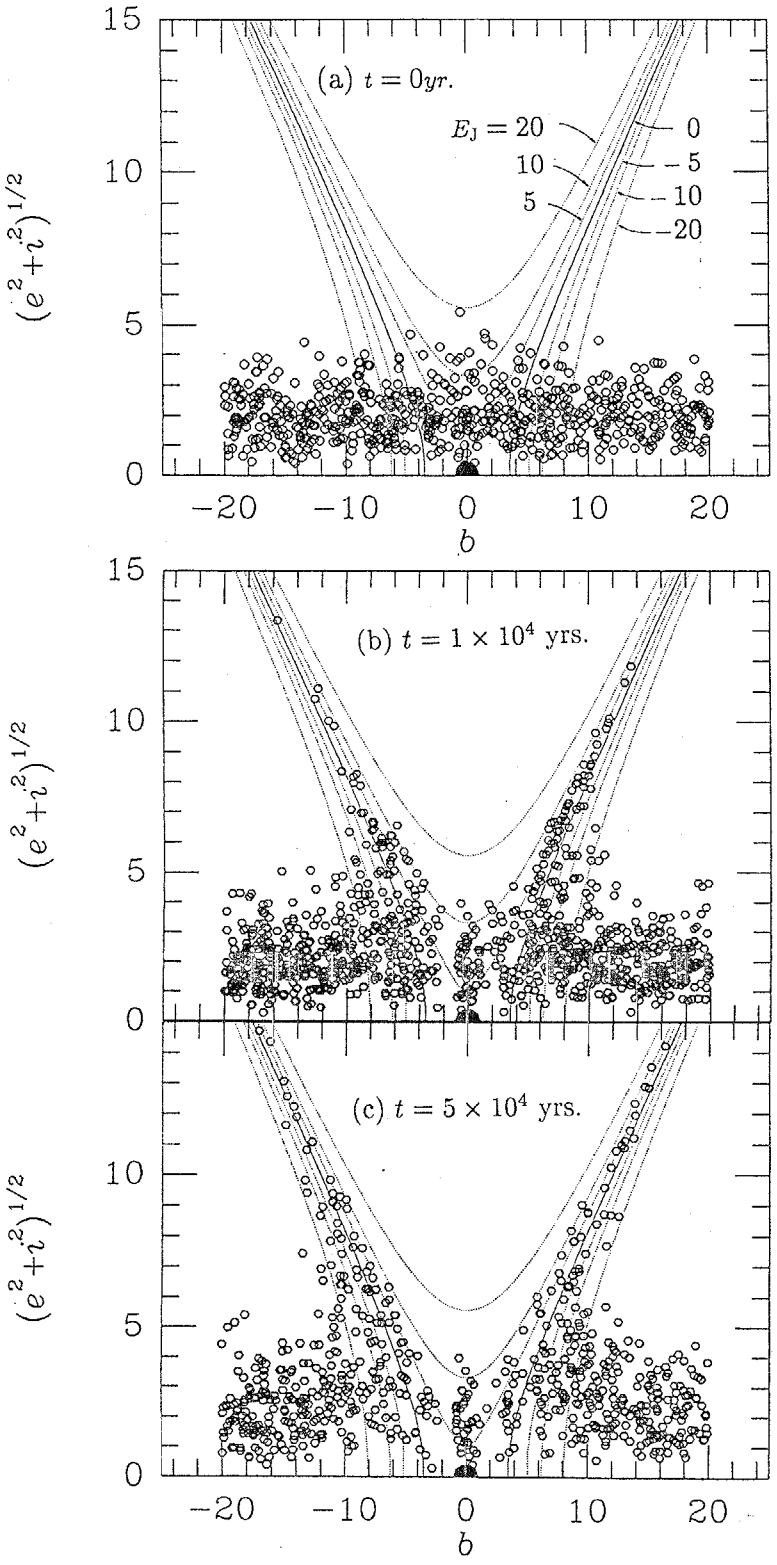

Fig. 8. The evolution of spatial and velocity distribution of 700 planetesimals with $m = 1 \times 10^{24}$g around a protoplanet with $M = 5 \times 10^{25}$g at 1 AU in the gas-free circumstance. Ordinates $(e^2 + i^2)^{1/2}$ express the magnitude of the random velocity and abscissas b express the radial position relative to the protoplanet. The protoplanet (large filled circle) is at the origin (*i.e.*, $b = 0$ and $e = i = 0$).

planetesimal is far from the protoplanet (*i.e.*, $r \gg 1$), which is given by (see Eq. (2.11))

$$E_{\rm J} = \frac{1}{2}(e^2 + i^2) - \frac{3}{8}b^2 + \frac{9}{2}. \tag{5.1}$$

In the scattering by a protoplanet, as mentioned in Section 2, the Jacobi energy $E_{\rm J}$ is conserved. Hence, in this gas-free case, planetesimals move along contours of $E_{\rm J}$ given by Eq. (5.1), except at the moment of close encounter ($r \lesssim 1$). Figure 8 shows that the scattering in general moves planetesimals along the lines in the direction that both $|b|$ and $(e^2 + i^2)^{1/2}$ increases. The effect of the scattering by the protoplanet is notable in the region $E_{\rm J} \geq 0$ since planetesimals with $E_{\rm J} \geq 0$ can approach the protoplanet closely. For larger t ($> 5 \times 10^4$ years), we obtain a qualitatively similar distribution with larger $(e^2 + i^2)^{1/2}$. [The random velocity $(e^2 + i^2)^{1/2}$ increases forever, since there is no dissipative process for the random velocity in this case.] Ida and Makino (1993) has already performed similar simulations of planetesimal-protoplanet system by N-body calculations. Our results are consistent with their results.

The planetesimals can enter the Hill sphere (the sphere with radius ha_M) of the protoplanet only if $E_{\rm J} > 0$ (e.g., Hayashi *et al.*, 1977). Thus, we define the "feeding zone" of the protoplanet as the region of $E_{\rm J} > 0$ in the above figures. Because of the conservation of $E_{\rm J}$, the planetesimals in feeding zone are not pushed out of the zone only due to the scattering by the protoplanet.

(ii) The case in the nebula gas

Next, we take account of the effect of the gas drag. The reduced Hill radius for $M = 5 \times 10^{25}$g is given by

$$h = (\frac{M}{3M_\odot})^{1/3} = 2.0 \times 10^{-3}. \tag{5.2}$$

In this case, the characteristic timescale of the gas drag T_0 is 1.3×10^6 years. To save the computation time, we take the value of T_0 to be smaller one, *i.e.*, $T_0 = 3.2 \times 10^5$ years, which corresponds to that we take larger $C_{\rm D}$ or larger $\rho_{\rm gas}$. This accelerates the evolution

of the planetesimal swarm due to the gas drag but does not change the course of the evolution. For the parameter η, we adopt a usual value 2×10^{-3}, given by Eq. (4.4).

We take the same initial distribution of planetesimals as those in the gas-free case (*i.e.*, Fig. 8(a)). The resultant spatial and velocity distributions at time $t = 1\times10^4, 5\times10^4$, and 4×10^5 years are plotted in Fig. 9 (a), (b), and (c), respectively. Owing to the gas drag force, e and i are kept low compared with the gas-free case. However, the most important result is that the planetesimals escape from the feeding zone of the protoplanet. The escape occurs with the help of gas drag as follows. In this case, the Jacobi energy $E_{\rm J}$ of each planetesimal is not conserved due to the gas drag. Then, planetesimals go across constant $E_{\rm J}$ curves. From Eq. (4.5), the ratio of the changes $\Delta(e^2 + i^2)^{1/2}/\Delta b$ due to the gas drag is obtained by $(e^2 + i^2)^{1/2}/(\eta/h)$, which is equal to $(e^2 + i^2)^{1/2}$ in this case $(h = \eta = 2\times10^{-3})$. On the other hand, the ratio along constant $E_{\rm J}$ curve takes the value $3b/4(e^2+i^2)^{1/2}$ which is reduced to $\pm\sqrt{3/4}$ for large $(e^2+i^2)^{1/2}$. The planetesimals in the feeding zone are scattered strongly by the protoplanet and obtain large random velocities e and i. Then, their ratios $\Delta(e^2 + i^2)^{1/2}/\Delta b$ become larger than those along constant $E_{\rm J}$ curves. As a result, $E_{\rm J}$ decreases due to gas drag. Since almost all the planetesimals with $E_{\rm J} > 0$ are scattered strongly by the protoplanet, they go out of the feeding zone of the protoplanet. This mechanism of the escape is explained more qualitatively as follows. Scattering by the protoplanet increase the differences in the semimajor axis between the planetesimals and the protoplanet as well as the random velocities. In spite of the increased differences in the semimajor axis, the planetesimals are still able to collide with the protoplanet since large random velocities mean large radial excursions. However, the gas drag reduces random velocities, *i.e.*, radial excursions, which makes the collision between planetesimals and the protoplanet impossible. Thus, planetesimals go out of the feeding zone of the protoplanet.

As pointed out in Section 4.3, in the presence of nebular gas, the protoplanet migrates to the sun due to the reaction of encounters with planetesimals and the gas drag.

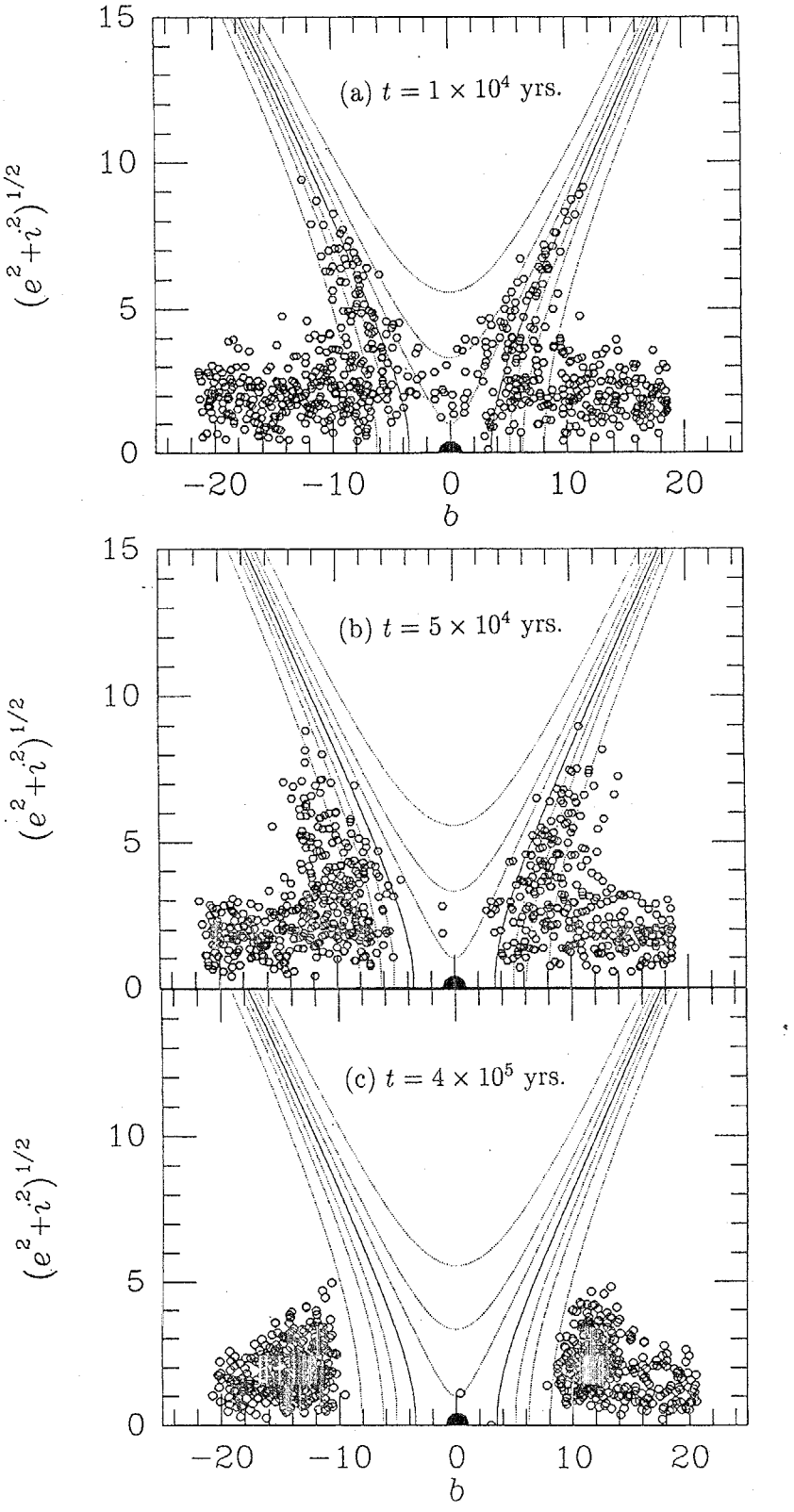

Fig. 9. The evolution of spatial and velocity distribution of planetesimals in the solar nebula. Conditions are the same as those in Fig. 8.

Figure 10 shows that the migration speed of the protoplanet $\dot{a}_M/ha_M$ of the simulation of Fig. 9. The migration speed is about 0.7×10^{-5} [years^{-1}], which is close to the migration speed due to the gas drag for planetesimals, which is evaluated from Eq. (4.5) as about 1×10^{-5} [years^{-1}], rather than that for the protoplanet, 0.3×10^{-5} [years^{-1}]. That is, the protoplanet migrates almost together with the planetesimal swarm. Actually, as seen from Fig. 9, the migration of the planetesimals relative to the protoplanet is little. This migration of the protoplanet is explained as follows. Due to the gas drag, the planetesimals in the region $b > 0$ approach to the protoplanet while those in $b < 0$ go away from the protoplanet. Then, the protoplanet scatters the planetesimals in $b > 0$ more strongly than those in $b < 0$. Due to the asymmetry of the reactions of the scatterings between $b > 0$ and $b < 0$, the protoplanet migrates toward the sun in order to cancel the asymmetry. Thus the protoplanet migrates together with the planetesimals.

As a result, the planetesimals in $b > 0$ cannot enter the feeding zone of the protoplanet, though planetesimals migrates to the sun due to the gas drag faster than the protoplanet do if only the migration due to gas drag is considered. In this manner, the planetesimals escape from the feeding zone of the protoplanet and most of them do not enter there again. If this spatial and velocity distribution is realized, the growth of the protoplanet will stop. Previously, it has been believed that the gas drag supplies planetesimals to the feeding zone of protoplanets by the differential migration speed (*e.g.*, Nakazawa *et al.* 1983, Ohtsuki *et al.*, 1988). However, our result shows the quite opposite effect of the gas drag.

5.2. Clean-up time of the planetesimals in the feeding zone

In the previous subsection, we showed that the protoplanet cleans up the planetesimals in the feeding zone ($E_J \geq 0$) with the help of the gas drag. Here we investigate the timescale taken to clean up the planetesimals in the feeding zone.

To see the manner of clean-up, we performed a more detailed simulation with 2000

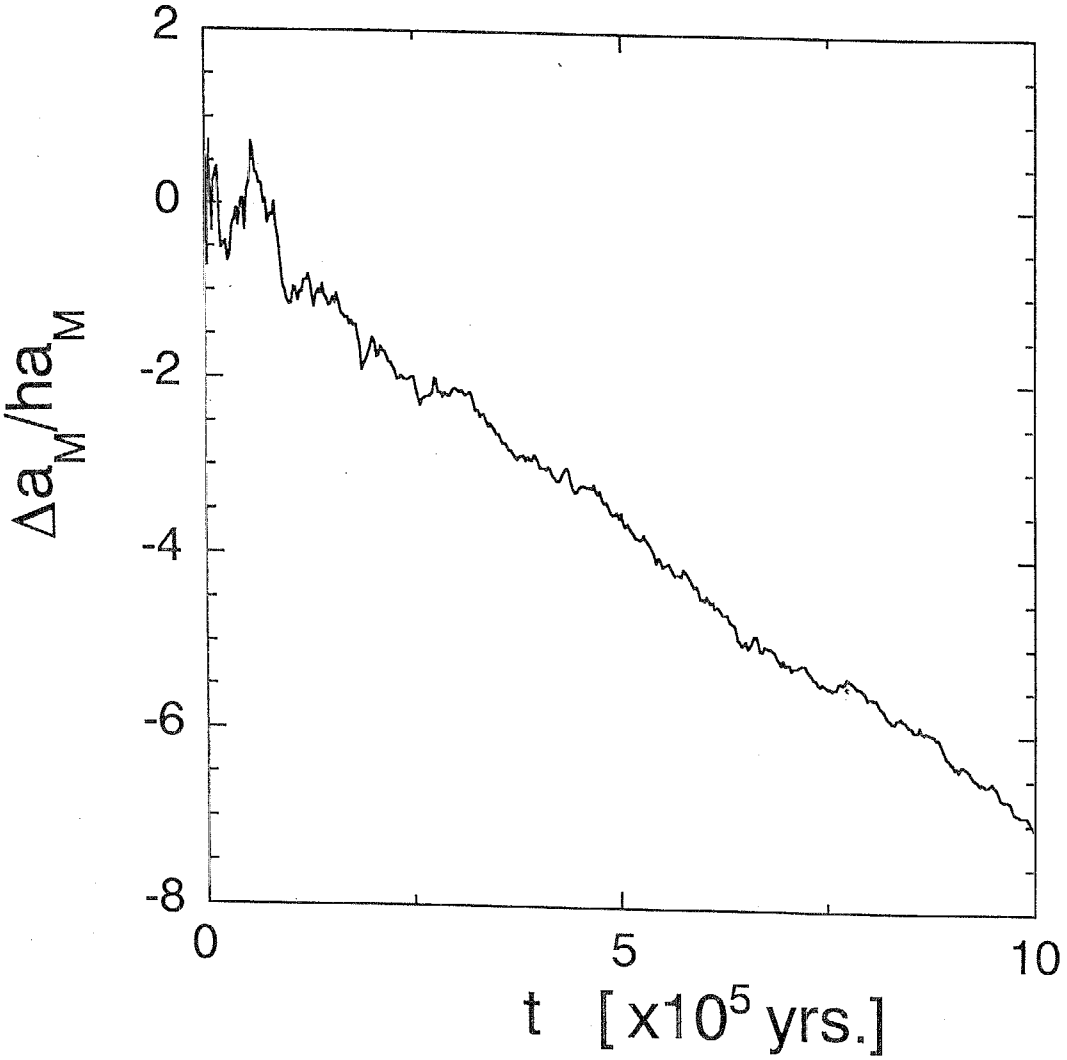

Fig. 10. The radial migration of the protoplanet. The vertical axis represents the deviation in semimajor axis a_M of the protoplanet from the initial position $a_{M,0}$, *i.e.*, $\Delta a_M = (a_M - a_{M,0})$.

planetesimals with $m = 5 \times 10^{23}$g and a protoplanet with $M = 4 \times 10^{25}$g. In this simulation, we adopted realistic parameter values: $\eta = 2 \times 10^{-3}$ and $T_0 = 1.3 \times 10^6$years. As the initial values of random velocities, we take $\langle e^2 \rangle^{1/2} = 2\langle i^2 \rangle^{1/2} = 6$, which are the equilibrium values balancing enhancement due to scatterings by the protoplanet with dissipation due to the gas drag at 1AU (Ida and Makino 1993).

In Fig. 11, we plot the spatial and velocity distributions of the planetesimals at time $t =$ (a)4×10^4, (b)8×10^4, and (c)2×10^5 years. The protoplanet cleans up the planetesimals in the feeding zone. In Fig. 12, we show the variation of the number of the planetesimals in the feeding zone. The number of the planetesimals in the feeding zone gradually decreases. We define the clean-up time $T_{\rm clean}$ by the time when this number becomes half of the initial value. From Fig. 12, we obtain the clean-up time $T_{\rm clean} = 7.7 \times 10^4$ years in this case.

Next, to examine the dependence of the clean-up time $T_{\rm clean}$ on T_0, we further performed simulations with various values of T_0, 6.5×10^5, 2.6×10^6, and 5.2×10^6 years, and obtained the clean-up time in the same way for each case. In each simulation, the initial dispersions $\langle e^2 \rangle^{1/2}$ and $\langle i^2 \rangle^{1/2}$ is determined so as to balance enhancement due to the scattering with dissipation due to the gas drag. The obtained results are summarized in Table I and plotted in Fig. 13. From Fig. 13, we obtain the dependence of the clean-up time $T_{\rm clean}$ on the characteristic time scale of the gas drag T_0 as:

$$T_{\rm clean} = 0.69 \left(\frac{T_0}{T_{\rm K}}\right)^{0.82} T_{\rm K}. \tag{5.3}$$

In the following, we prove that the clean-up time $T_{\rm clean}$ is no other than the dissipation timescale $T_{\rm gas}$ due to the gas drag defined by

$$T_{\rm gas} \equiv \frac{e}{\dot{e}_{\rm gas}} \simeq \frac{T_0}{\langle e^2 \rangle^{1/2}}, \tag{5.4}$$

where we used Eq. (4.2) for $\dot{e}_{\rm gas}$. As mentioned above, the dispersion $\langle e^2 \rangle^{1/2}$ is determined by the balance between enhancement due to scatterings by the protoplanet and dissipation due to the gas drag. The enhancement timescale due to scatterings by the

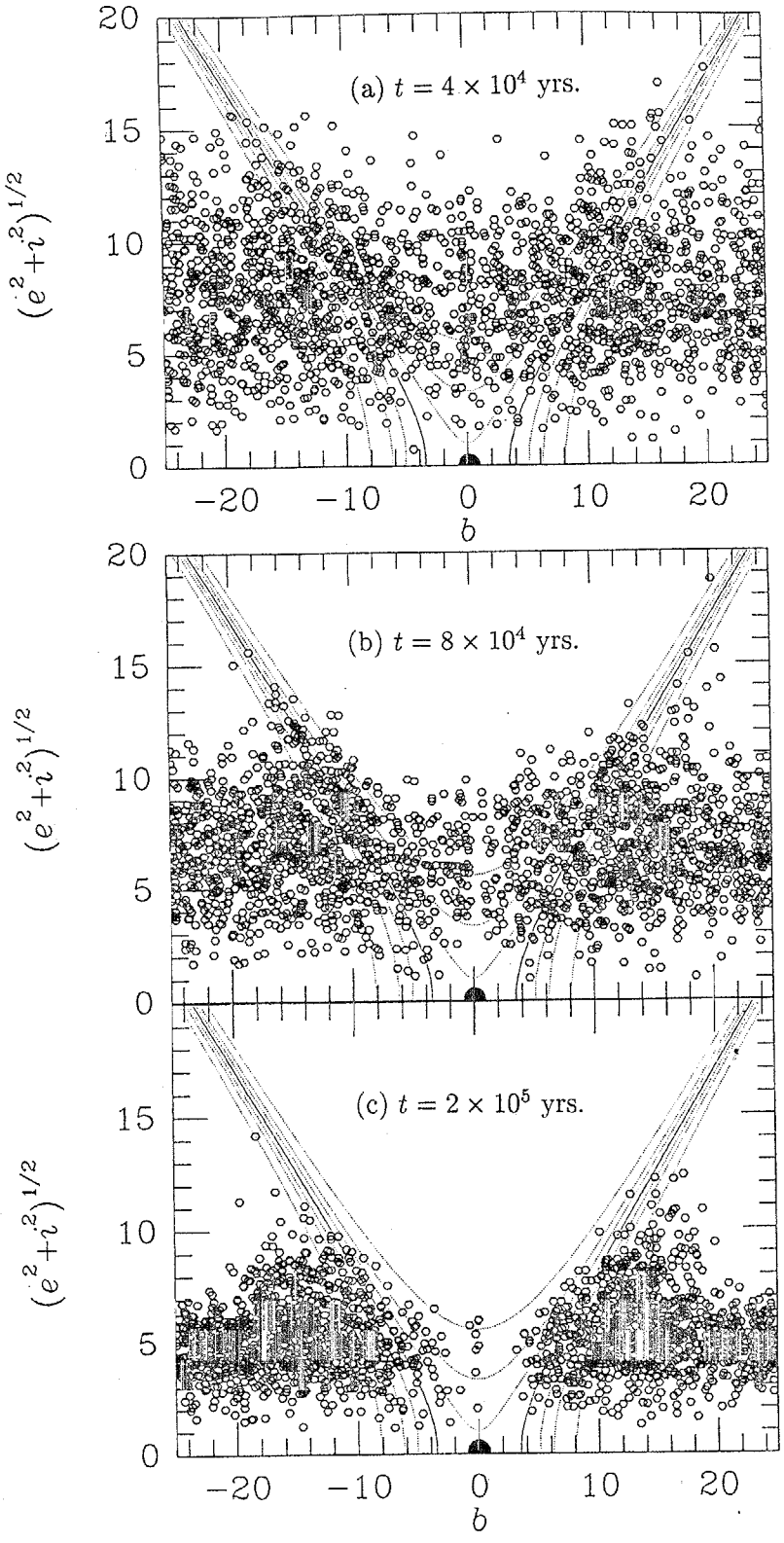

Fig. 11. The spatial and velocity distributions of the 2000 planetesimals with $m = 5 \times 10^{23}$g around a protoplanet with $M = 4 \times 10^{25}$g at 1AU (a)$t = 4 \times 10^4$ years, (b)8×10^4 years, and (c)2×10^5 years.

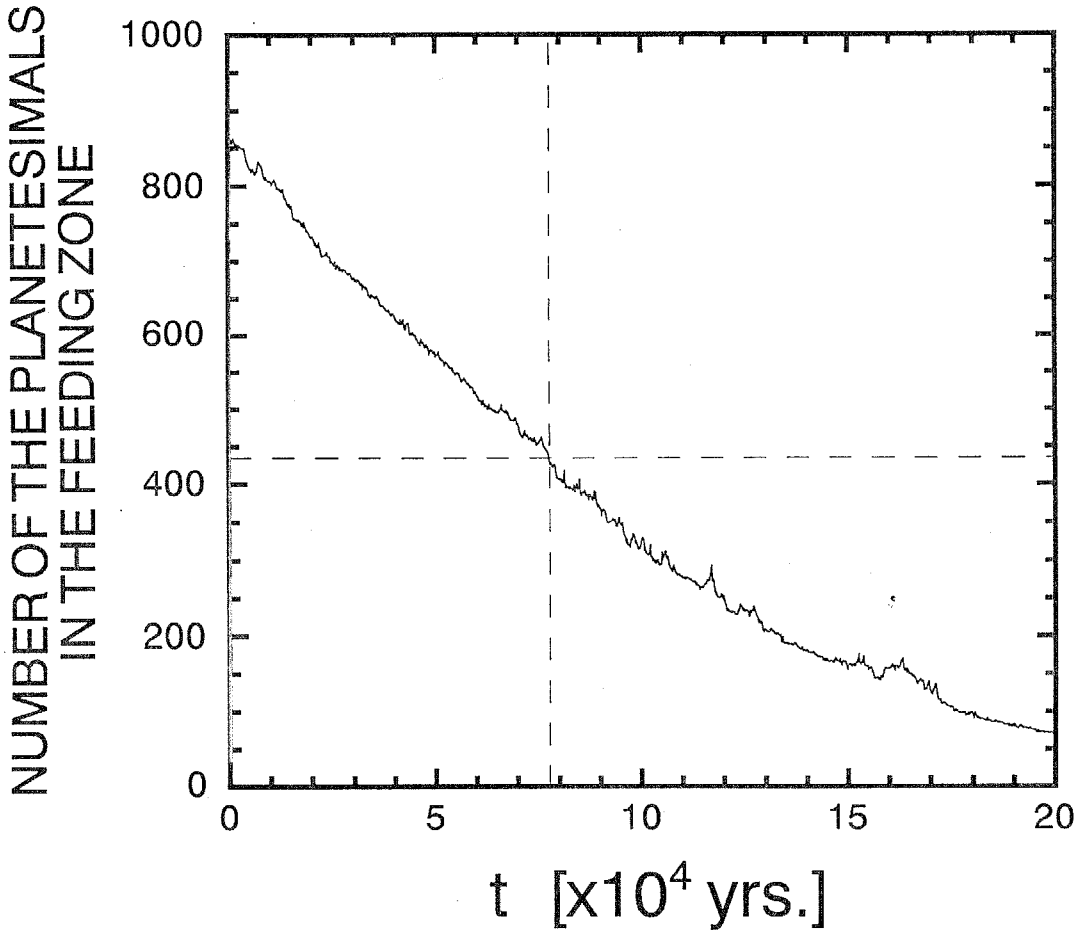

Fig. 12. The variation of the number of the planetesimals in the feeding zone. The number of the planetesimals in the feeding zone gradually decreases and becomes half at time $t = 7.7 \times 10^4$ years.

Table I.

Dependence of the clean-up time $T_{\rm clean}$ on T_0.

T_0 [$\times 10^6 T_{\rm K}$]	$T_{\rm clean}$ [$\times 10^5 T_{\rm K}$]
0.65	0.39
1.3	0.77
2.6	1.2
5.2	2.2

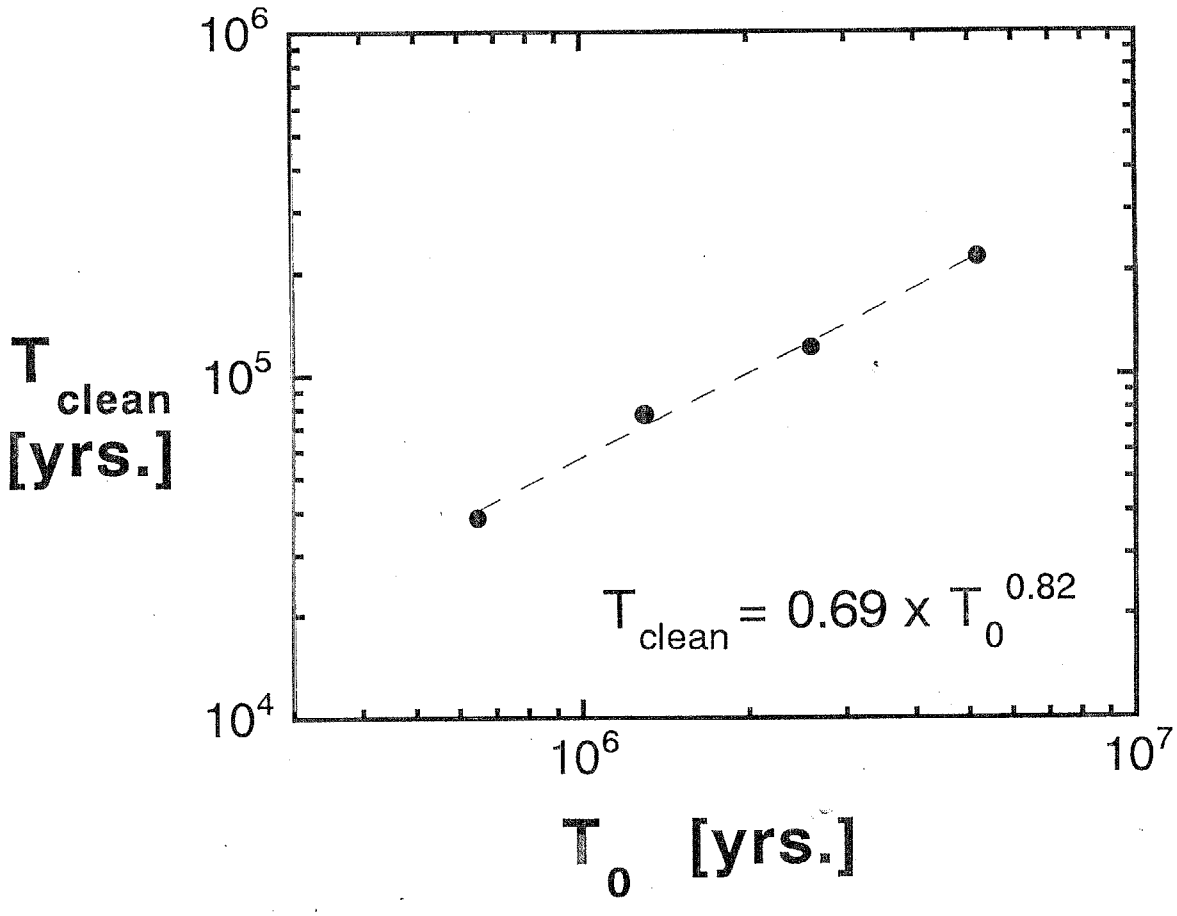

Fig. 13. The dependence of the clean-up time $T_{\rm clean}$ on the characteristic time scale of the gas drag T_0.

protoplanet is proportional to $\langle e^2 \rangle^{5/2}$ (see Ida and Makino, 1993). Balancing this enhancement time scale with $T_{\rm gas}$ (5.4), we see that $\langle e^2 \rangle^{1/2}$ is proportional to $T_0{}^{1/6}$. Since $\langle e^2 \rangle^{1/2} = 6$ for $T_0 = 1.3 \times 10^6 T_{\rm k}$, $\langle e^2 \rangle^{1/2}$ is given by

$$\langle e^2 \rangle^{1/2} \simeq 6 (\frac{T_0}{1.3 \times 10^6 T_{\rm K}})^{1/6} \simeq 0.6 (\frac{T_0}{T_{\rm K}})^{1/6}. \tag{5.5}$$

Substituting Eq. (5.5) to Eq. (5.4), we finally obtain

$$T_{\rm gas} \simeq 2 (\frac{T_0}{T_{\rm K}})^{5/6} T_{\rm K}. \tag{5.6}$$

Comparing Eq. (5.6) with Eq. (5.3), we find $T_{\rm clean} \simeq T_{\rm gas}/3$. This result is reasonable because the clean-up of the planetesimals occurs owing to the gas drag. So far, we have considered at 1AU. We can consider at other heliocentric distance in a quite similar way. We found that the relation $T_{\rm clean} \sim T_{\rm gas}$ holds everywhere. Consequently, we conclude that most of the planetesimals in the feeding zone are cleaned up within the time scale $T_{\rm gas}$. Using Eqs. (4.5), (5.4), and (5.5), we have $T_{\rm gas}$ as

$$T_{\rm gas} \simeq 6 \times 10^5 C_{\rm D}^{-5/6} (\frac{m}{M})^{5/18} (\frac{a}{1{\rm AU}})^{35/24} T_{\rm K}. \tag{5.7}$$

5.3. The generality of the clean-up time

To make clear the generality of the above result, we examine the dependence of the result on other parameters. In our simulation, there are mainly five independent parameters: the number of planetesimals N, the mass ratio M/m, the reduce Hill radius $h \equiv (M/M_\odot)^{1/3}$, the characteristic time scale of the gas drag T_0, and $\tilde{\eta} \equiv \eta/h$. We have already examined the T_0-dependence. Furthermore, in our simulation, the reduced Hill radius h appears only through the synodic period $T_{\rm s} \propto 1/h$, $T_0 \propto 1/h$, and $\tilde{\eta}$. If we normalize time by $T_{\rm K}/h$, $T_{\rm s}$ and T_0 become independent of h. Thus, the h-dependence can be absorbed by the $\tilde{\eta}$-dependence. We examine the dependence on the other parameters $\tilde{\eta}$, N, and M/m. We will show the clean-up time is almost independent of these parameters.

First, we examine the $\tilde{\eta}$-dependence. To do this, we performed the simulations for various value of $\tilde{\eta}$ (=1, 5, and, 10) with other parameters fixed; we put $M = 40m = 4 \times 10^{25}$g, $N = 800$, and $T_0 = 3.2 \times 10^5$years. In Fig. 14, we showed the time-variation of the number of planetesimals in the feeding zone for each case. Figure 14 indicates that the evolution does not depend on $\tilde{\eta}$ as long as $\tilde{\eta} \leq 5$. But, for $\tilde{\eta} = 10$ much more planetesimals remain in the feeding zone than for $\tilde{\eta} \leq 5$. This result for $\tilde{\eta} = 10$ is explained as follows. When $\tilde{\eta}$ is large enough, the ratio of changes $\Delta e/\Delta b \simeq e/\tilde{\eta}$ due to the gas drag can be smaller than $\sqrt{3/4}$. Then, in the region $b > 0$, the Jacobi energy of planetesimals increase rather than decrease and the planetesimals can enter the feeding zone from the side $b > 0$.

The parameter $\tilde{\eta}$ become large enough only when $M \lesssim 10^{23}$g (*i.e.*, $h \lesssim 10^{-3}$). However, we consider the case where the gravity of the protoplanet is sufficiently strong, the case with $M \gtrsim 10^{23}$g. Hence, in the case we now consider, the clean-up of the planetesimals in the feeding zone occurs independent of $\tilde{\eta}$.

Next, we examine the dependence on N and M/m. We calculated for two mass ratios $M/m = 40$ and 100 with the total mass ratio Nm/M and M fixed ($Nm/M = 20$ and $M = 4 \times 10^{25}$g). This means the constant initial surface density because we fixed the radial range of the initial distribution of planetesimals $\Delta a = 40h$ AU. In Fig. 15, we showed the fraction of planetesimals remaining in the feeding zone for the two cases. Figure 15 shows that the evolution is independent of the mass ratio M/m. Moreover, we performed simulations for various value of the total mass Nm/M with $N = 800$, $M = 4 \times 10^{25}$g, and $\Delta a = 40h$ AU. That is, we change the initial surface density of planetesimals in the feeding zone with the mass of the protoplanet M fixed. In Fig. 16, the number of planetesimals in the feeding zone is presented for each case. The obtained number slightly depend on the total mass ratio but the protoplanet cleans up the planetesimals in the feeding zone in almost the same time scale for all the cases. Consequently, it is concluded that the clean-up by the protoplanet is a very general phenomenon when its gravity is sufficiently strong and the nebula gas exists.

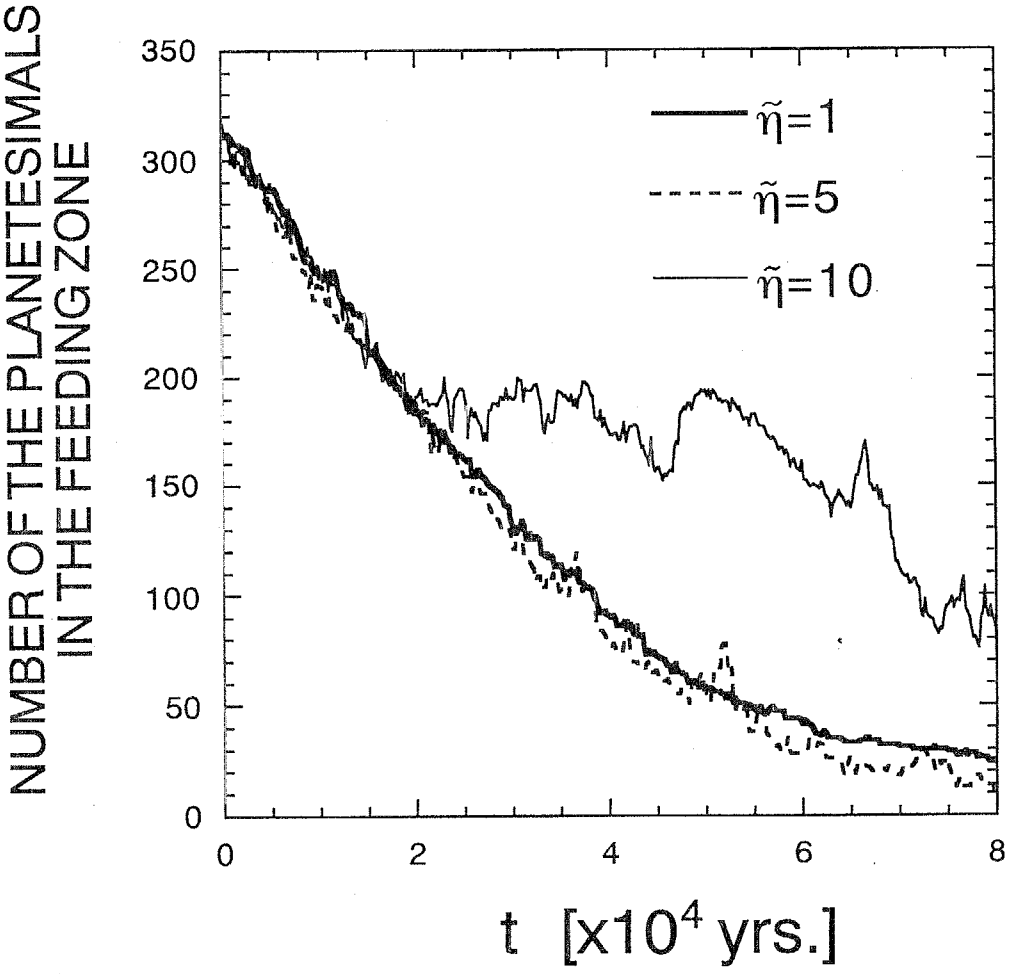

Fig. 14. The time-variation of the number of planetesimals in the feeding zone for $\tilde{\eta}$ =1, 5, and, 10. The evolution does not depend on $\tilde{\eta}$ when $\tilde{\eta} \leq 5$. For $\tilde{\eta} = 10$, a considerable number of planetesimals remain in the feeding zone.

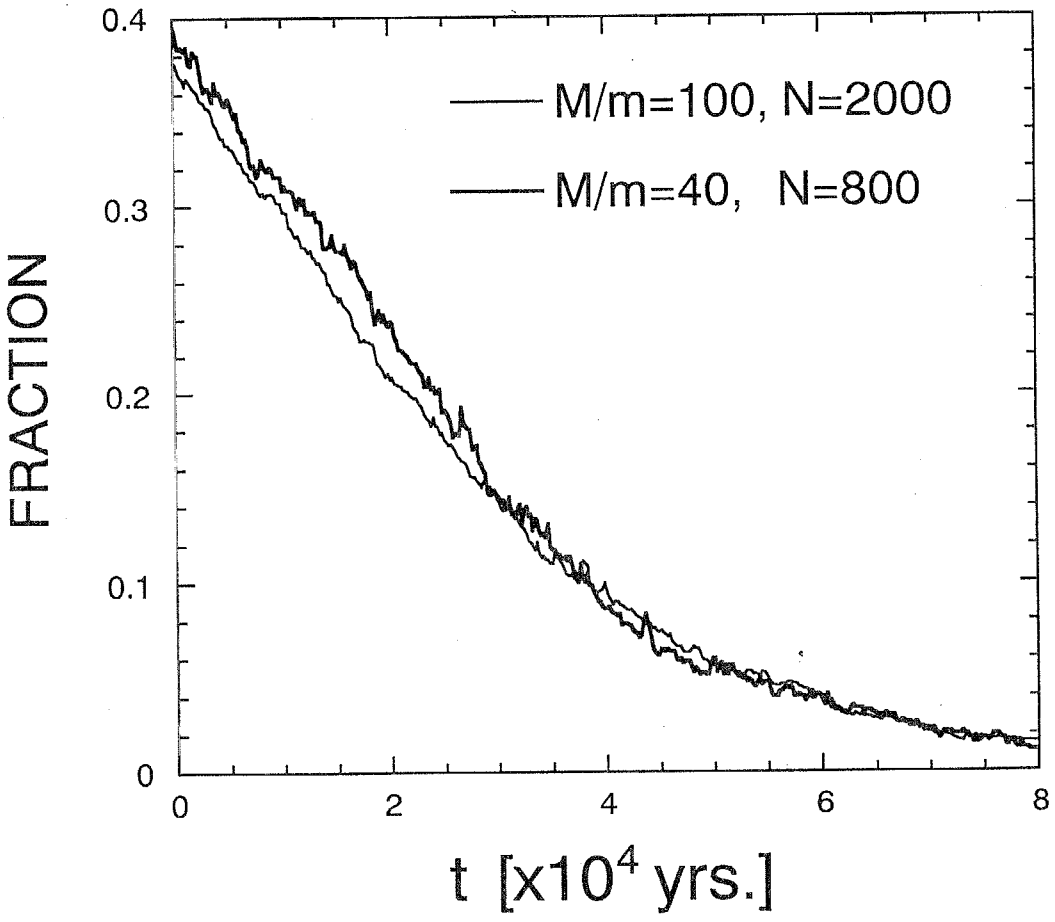

Fig. 15. The fraction of planetesimals in the feeding zone for two mass ratios fixed as $M/m = 40$ and 100 with the total mass ratio $Nm/M = 20$. The evolution is independent of the mass ratio M/m if the total mass ratio Nm/M is fixed.

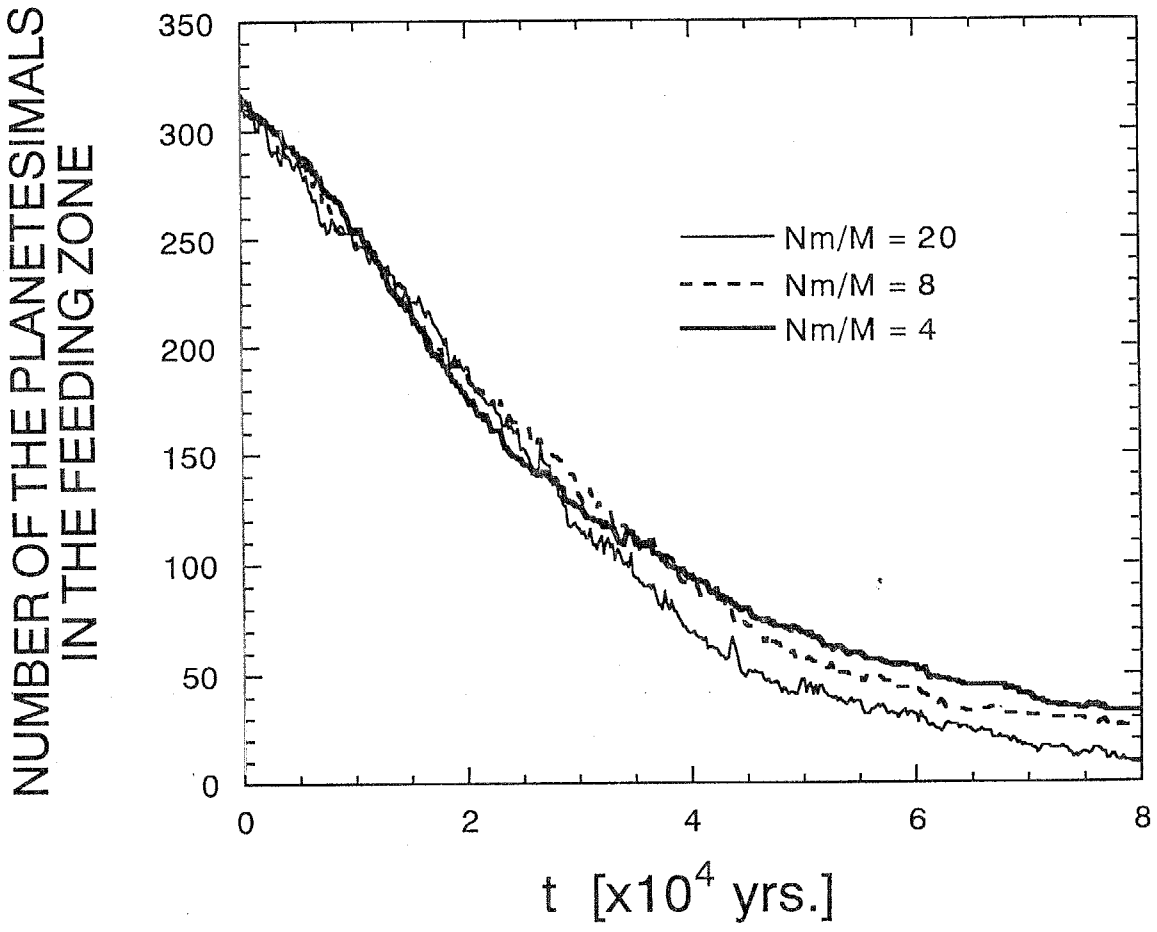

Fig. 16. The dependence on the total mass ratio Nm/M. The number of planetesimals in the feeding zone slightly depend on the total mass ratio.

6 Conclusion and Discussion

In the gas-free circumstance, the scattering by a protoplanet enhances random velocities e and i of the neighboring planetesimals to relatively high values and makes considerable nonuniformity in the spatial distribution of planetesimals, if M/m becomes larger than a critical value [$M/m \geq 50\,(\mathrm{m}/10^{23}\mathrm{g})^{-2/5}$ at 1AU, $M/m \geq 100\,(\mathrm{m}/10^{24}\mathrm{g})^{-2/5}$ at 5AU] (Ida and Makino 1993). Since the scattering does not push the planetesimals out of the feeding zone (the region with $E_\mathrm{J} \geq 0$) because of the conservation of E_J, it does not inhibit further growth of the protoplanet.

However, planets should have grown in the nebula gas in great part of their formation. Since the gas drag effect does not conserve E_J, it is essential to take into account the gas drag in order to know the realistic spatial distribution of planetesimals. We simulated the long term evolution of the spatial and velocity distribution of planetesimals around a protoplanet, taking account of the gas drag. In our simulation, we neglected scattering between planetesimals, since we considered the late accretion stage. The results are as follows:

1. The gas drag always decreases the Jacobi energy of the planetesimals which were scattered strongly by the protoplanet and, as a result, the scattered planetesimals go out of the feeding zone. That is, the protoplanet cleans up the planetesimals in the feeding zone with the help of the gas drag. If the planetesimals in the feeding zone are completely cleaned up, the growth of the protoplanet will stop.

2. The clean-up of the planetesimals occurs in the dissipation time scale due to the gas drag T_gas, given by

$$T_\mathrm{gas} \simeq 6 \times 10^5 C_\mathrm{D}^{-5/6} \left(\frac{m}{M}\right)^{5/18} \left(\frac{a}{1\mathrm{AU}}\right)^{35/24} T_\mathrm{K}. \tag{6.1}$$

Since the growth time of the protoplanet is always much larger than T_gas (Ohtsuki *et al.*, 1993), the protoplanet finishes clean-up of planetesimals in the feeding zone before the protoplanet feeds them.

It has been expected that the gas drag moves planetesimals radially and supplies planetesimals to the feeding zone so that planet growth is accelerated (Nakagawa *et al.*, 1983; Ohtsuki *et al.*, 1988). However, our result shows opposite trend of the gas drag as effect.

Our result implies that runaway growth stops if the mass ratio M/m becomes large, as long as in the nebula gas. This raises "the growth time problem of Jovian-type planets" again. In the below, we consider the effects we have not included so far and examine the possibility which relieves the above difficulties.

The first is interactions between planetesimals. The diffusion due to interactions between planetesimals makes their distribution uniform. However, the smoothing due to interactions between planetesimals is effective only when the interactions between planetesimals are more effective than the gravity of the protoplanet, *i.e.*, $M/m \leq$ 50-100. Hence, it cannot remove the above difficulty.

The second effect is the mass distribution of planetesimals. Radial migration speed due to the gas drag depends on the planetesimal mass. As a result, a planetesimal swarm with mass distribution can diffuse radially. To examine the effect, we performed a preliminary simulation taking account of the mass distribution of planetesimals. We calculated orbital evolutions of 200 planetesimals with $m_1 = 1 \times 10^{24}$g and 400 planetesimals with $m_2 = m_1/8$ around a protoplanet with $M = 50m_1$. In Fig. 17, we showed the time evolution of the spatial and velocity distributions of planetesimals. Filled circles and opened ones represent planetesimals m_1 and m_2, respectively. This preliminary result suggests that the mass distribution is not so effective to inhibit the clean-up. To conclude the effect of the mass distribution, however, further investigations are needed.

If the gas drag force is so strong that $T_{\rm gas} \sim T_{\rm s}$, planetesimals can enter the feeding zone of the protoplanet during the synodic time. Then, runaway growth of the protoplanet may be able to continue. The case of the strong gas drag is realized for very small planetesimals (*i.e.*, $m \lesssim 10^{15}$g). It is likely that such small planetesimals are created by collisional disruption. In the vicinity of a protoplanet, the random velocities e and i of

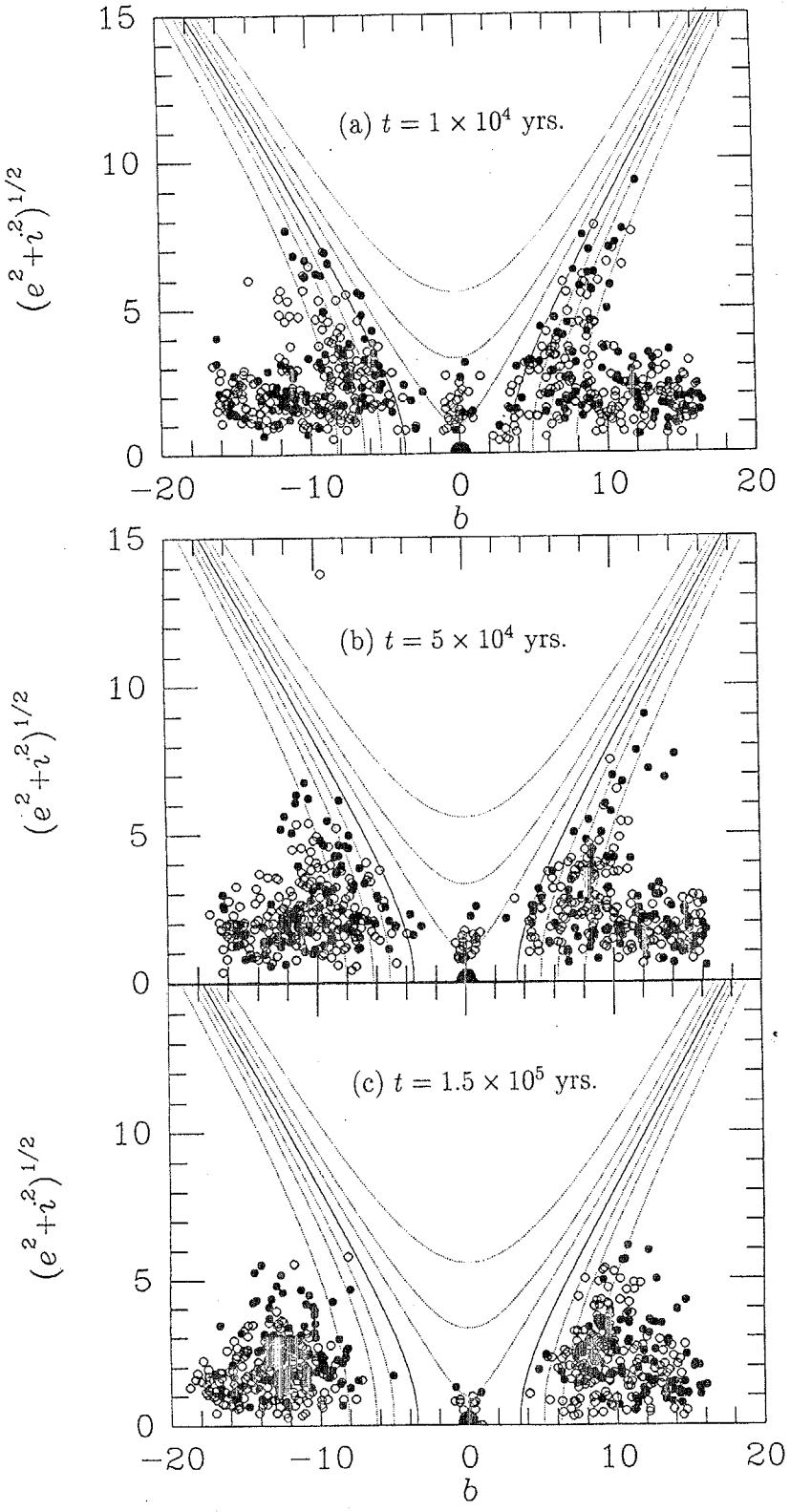

Fig. 17. The time evolution of the spatial and velocity distributions of planetesimals with different masses. We calculated 200 planetesimals $m_1 = 1 \times 10^{24}$g and 400 planetesimals with $m_2 = m_1/8$ around a protoplanet with $M = 50m_1$. Filled circles and opened ones represent planetesimals m_1 and m_2, respectively.

planetesimals are largely enhanced by the protoplanet as seen in Fig. 9. If the random velocities exceed the escape velocity from the surface of planetesimals, planetesimals are disrupted by their mutual collisions (Wetherill and Stewart, 1993).

Another probable effect of inhibiting the clean-up is that some protoplanets exist radially close to one another (*e.g.*, the radial space between two protoplanet Δb is less than ~ 10). In such a case, since planetesimals could be influenced by two protoplanets, planetesimals migrate rather randomly and substantial amount of planetesimals may exist in the feeding zones. Then, the runaway growth of the protoplanets is possible also after scatterings by protoplanets become more effective than those between planetesimals.

In order to clarify how the protoplanet grow in the late stage, further investigations of disruption of planetesimals and spacing of protoplanets are needed. Whatever growth of protoplanet may occur, the problem of the cleanup by protoplanets is the essential and unavoidable one in the planetary formation.

Acknowledgments

The author is indebted to Dr. Sigeru Ida for valuable advice. The author is also indebted to Dr. Kiyoshi Nakazawa for valuable comments and criticisms. He thanks Dr. Hiroaki Emori for fruitful discussions and Ms. Kei Kudo for help in preparing the manuscript.

Appendix

We describe the way of deriving the closest point $\boldsymbol{r}_{\rm min}$ and the velocity at the closest point $\boldsymbol{v}_{\rm min}$ of the Keplerian orbit around the sun. If the time at the closest point $t_{\rm min}$ is given, we can obtain $\boldsymbol{r}_{\rm min}$ and $\boldsymbol{v}_{\rm min}$ from Eqs. (2.6) and (2.7), respectively. The accurate values of $\boldsymbol{r}_{\rm min}$ and $\boldsymbol{v}_{\rm min}$ are needed for Regime 1 and 3 (*i.e.*, for relatively close encounters) to calculate scattering matrices while they are not for Regime 2. Hence, we only have to obtain the time $t_{\rm min}$ for relatively close encounters, $r_{\rm min} < v_{\rm min}/3$. We divide these encounters into the following three cases: (i) $b < e$, (ii) $b \geq e$ and $e \gg 1$, and (iii) $b \geq e$ and $e \sim 1$. For each case, we explain the way of deriving $t_{\rm min}$ below.

(i) Case of $b < e$

In this case, we derive $t_{\rm min}$, following Nakazawa *et al.* (1989). First, we seek "collision orbits " which pass through the origin $(x, y, z) = (0, 0, 0)$. From Eq. (2.6) with $\lambda = 0$, phases (τ, ω) of collision orbits, which we denote by $(\tau_{\rm coll}, \omega_{\rm coll})$, satisfy

$$\begin{cases} b - e\cos(t_{\rm coll} - \tau_{\rm coll}) = 0, \\ -\frac{3}{2}bt_{\rm coll} + 2e\sin(t_{\rm coll} - \tau_{\rm coll}) = 0, \\ i\sin(t_{\rm coll} - \omega_{\rm coll}) = 0, \end{cases} \tag{A.1}$$

where $t_{\rm coll}$ is collision time. From Eq. (A.1), we have four sets of $(t_{\rm coll}, \tau_{\rm coll}, \omega_{\rm coll})$ $(-\pi < \tau_{\rm coll} < \pi, -\pi < \omega_{\rm coll} < \pi)$ as

$$(t_{\rm coll}, \tau_{\rm coll}, \omega_{\rm coll}) = \begin{cases} (t^*, \tau^*, \omega^*), \quad (t^*, \tau^*, \omega^* - \pi), \\ (-t^*, -\tau^*, -\omega^*), \quad \text{and} \quad (-t^*, -\tau^*, -\omega^* + \pi), \end{cases} \tag{A.2}$$

where

$$\begin{cases} t^* = \dfrac{4}{3}\sqrt{(\dfrac{e}{b})^2 - 1}, \\ \tau^* = t^* - |\cos^{-1}(\dfrac{b}{e})|, \\ \omega^* = t^*. \end{cases} \tag{A.3}$$

Since we consider relatively close encounter orbits, their phases (τ, ω) differ from $(\tau_{\rm coll}, \omega_{\rm coll})$ only slightly. We define infinitesimals,

$$\begin{cases} \eta = \tau - \tau_{\rm coll}, \\ \zeta = \omega - \omega_{\rm coll}, \\ \xi = t - t_{\rm coll}. \end{cases} \tag{A.4}$$

We expand Eq. (2.6) with the above infinitesimals around the collision orbit. Using Eq. (A.1) we obtain

$$\begin{cases} x = e\sin(t_{\rm coll} - \tau_{\rm coll})(\xi - \eta) \quad + O(\epsilon^2), \\ y = \dfrac{b}{2}(\xi - 4\eta) \quad + O(\epsilon^2), \\ z = i(\xi - \zeta) \quad + O(\epsilon^2), \end{cases} \tag{A.5}$$

where ϵ is infinitesimal of the order of ξ, η, and ζ. Neglecting the third or higher order terms, we have the square of distance at $t = t_{\rm coll} + \xi$ as

$$\begin{aligned} r^2 &= x^2 + y^2 + z^2 \\ &= (e^2 + i^2 - \frac{3}{4}b^2)\xi^2 - 2(e^2\eta + i^2\zeta)\xi + (e^2 + 3b^2)\eta + i^2\zeta^2. \end{aligned} \tag{A.6}$$

The distance r takes the minimum value at $t = t^{(0)}_{\rm min} \equiv t_{\rm coll} + \xi_{\rm min}$, which is given in an accuracy of the order ϵ by

$$t_{\rm min}^{(0)} = t_{\rm coll} + \xi_{\rm min} = t_{\rm coll} + \frac{e^2(\tau - \tau_{\rm coll}) + i^2(\omega - \omega_{\rm coll})}{e^2 + i^2 - \frac{3}{4}b^2}. \tag{A.7}$$

From Eq.(A.6), the minimum distance $r_{\rm min}^2$ is approximately given by

$$r_{\rm min}^2 = \frac{9}{4}(\tau - \tau_{\rm coll})^2 + i^2(\omega - \omega_{\rm coll})^2 - \frac{[3/4b^2(\tau - \tau_{\rm coll}) + i^2(\omega - \omega_{\rm coll})^2]^2}{e^2 + i^2 - \frac{3}{4}b^2} + O(\epsilon^3). \tag{A.8}$$

Substituting Eq. (A.7) into Eq. (A.5), we can also obtain $\boldsymbol{r}_{\rm min}$ and $\boldsymbol{v}_{\rm min}$ ($\equiv \dot{\boldsymbol{r}}_{\rm min}$). Then we have $v_{\rm min}^2$ as

$$v_{\rm min}^2 = e^2 + i^2 - \frac{3}{4}b^2 \quad + O(\epsilon). \tag{A.9}$$

These obtained values of $t_{\rm min}$, $r_{\rm min}$, and $v_{\rm min}$ are not accurate enough especially for Regime 3. Thus we further perform following procedures to obtain more accurate value of $t_{\rm min}$. These procedures are equivalent to taking account of higher order terms of ϵ in Eq. (A.7).

The position $\boldsymbol{r}^{(0)}$ and velocity $\boldsymbol{v}^{(0)}$ at $t = t_{\rm min}^{(0)}$ is defined by substituting $t_{\rm min}^{(0)}$ into Eqs. (2.6) and (2.7):

$$\boldsymbol{r}^{(0)} \equiv \boldsymbol{r}_{\rm sun}(t_{\rm min}^{(0)}), \quad \boldsymbol{v}^{(0)} \equiv \dot{\boldsymbol{r}}_{\rm sun}(t_{\rm min}^{(0)}). \tag{A.10}$$

Using $\boldsymbol{r}^{(0)}$ and $\boldsymbol{v}^{(0)}$, we approximately obtain the orbit $\boldsymbol{r}_{\rm sun}$ around $t = t_{\rm min}^{(0)}$ as

$$\boldsymbol{r}_{\rm sun} = \boldsymbol{r}^{(0)} + \boldsymbol{v}^{(0)}(t - t_{\rm min}^{(0)}). \tag{A.11}$$

Then the square distance $|\boldsymbol{r}_{\rm sun}|^2$ is given by

$$|\boldsymbol{r}_{\rm sun}|^2 = |\boldsymbol{r}^{(0)}|^2 + 2(\boldsymbol{r}^{(0)} \cdot \boldsymbol{v}^{(0)})(t - t_{\rm min}^{(0)}) + |\boldsymbol{v}^{(0)}|^2 (t - t_{\rm min}^{(0)})^2 \tag{A.12}$$

This distance $|\boldsymbol{r}_{\rm sun}|^2$ takes the minimum value at $t = t_{\rm min}^{(1)}$, which is given by

$$t_{\rm min}^{(1)} = t_{\rm min}^{(0)} - \frac{\boldsymbol{r}^{(0)} \cdot \boldsymbol{v}^{(0)}}{|\boldsymbol{v}^{(0)}|^2} \tag{A.13}$$

Consequently, using Eqs. (A.10) and (A.13), we can obtain more accurate value $t_{\rm min}^{(1)}$ for the closest time than $t_{\rm min}^{(0)}$. Furthermore, iterating the above procedures, we can obtain a sufficiently accurate value. Then, substituting $t_{\rm min}^{(1)}$ into Eqs. (2.6) and (2.7), we can obtain $\boldsymbol{r}_{\rm min}$ and $\boldsymbol{v}_{\rm min}$ with a good accuracy.

(ii) Case of $b \geq e$ and $e \gg 1$

In this case, we cannot use the method mentioned above since no collision orbits exist. Thus we introduce another method adequate for this case. When $b > 1.1e$ and $e \gg 1$, all orbits belong to Regime 2. Then $t_{\rm min}$ is not necessary. Hence, we consider the case of $e \leq b \leq 1.1e$ and $e \gg 1$. When the orbit passes close to the origin, each component of position must be small. Since $b \sim e$, as seen from Eq. (2.6), the x-component becomes small when $t - \tau \ll 1$. Furthermore, when $t - \tau \ll 1$, the y-component of position around the closest approach is given by

$$y = (2e - \frac{3}{2}b)t - 2e\tau \tag{A.14}$$

In the zeroth approximation, we define $t_{\rm min}$ so that $y = 0$:

$$t_{\rm min}^{(0)} = \frac{2e\tau}{2e - 3b/2} \tag{A.15}$$

In order to obtain more accurate value of $t_{\rm min}$, we perform the same procedures as Case (i). That is, we use Eqs. (A.10) and (A.13) and iterate them. Then we can obtain $t_{\rm min}$ with a good accuracy.

(iii) Case of $e \sim 1$

In this case, inclination i is much larger than unity because $(e^2 + i^2)^{1/2} \gg 1$. For a close encounter orbit, the time at the closest point is roughly given by ω or $\omega \pm \pi$ since $z = i \sin(t - \omega) \simeq 0$ then. Hence, we put $t_{\min} = \omega$ or $\omega \pm \pi$ in the zeroth approximation. Among the three values of $t_{\min}$, we choose the value which gives the minimum distance. In order to obtain more accurate value of $t_{\min}$, we must iterate Eqs. (A.10) and (A.13).

References

Adachi, I., C. Hayashi, and K. Nakazawa 1976. The gas drag effect on the elliptical motion of a solid body in the primordial solar nebula. *Prog. Theor. Phys.* **56**, 1756-1771.

Hasegawa, M. and K. Nakazawa 1990. Distant encounter between Keplerian particles. *Astron. Astrophys.* **227**, 619-627.

Hayashi, C. 1981. Structure of the solar nebula, growth and decay of magnetic fields and effects of magnetic and turbulent viscosities on the nebula. *Prog. Theor. Phys. Suppl.* **70**, 35-53.

Hayashi, C., K. Nakazawa, and I. Adachi 1977. Long term behavior of planetesimals and the formulation of the planets. *Publ. Astro. Soc. Japan* **29**, 163-196.

Hayashi, C., K. Nakazawa, and Y. Nakagawa, 1985. Formation of the solar System. in *Protostars and Planets II* (D.C. Black and M. S. Mathews, Eds.), pp.1100-1153. Univ. of Arizona Press, Tucson.

Hénon, M. and J. M. Petit 1986. Series expansions for encounter-type solutions of Hill's problem. *Celestial Mech.* **38**, 67-100.

Ida, S. 1990. Stirring and dynamical friction rates of planetesimals in the solar gravitational field. *Icarus* **88**, 129-145.

Ida, S. and J. Makino 1992. N-body simulation of gravitational interaction between planetesimals and a protoplanet. II. Dynamical friction. *Icarus* **98**, 28-37.

Ida, S. and J. Makino 1993. Scattering of planetesimals by a protoplanet: slowing down of runaway growth. *Icarus* **106**, 210-227.

Ida, S., E. Kokubo, and J. Makino 1993. The origin of anisotropic velocity dispersion of particles in a disc potential. *Mon. Not. R. Astron. Soc.* **263**, 875-889.

Landau, L.D. and E.M. Lifshitz 1957. *Mechanics* (Pergamon Press, London).

Mizuno, H., K. Nakazawa, and C. Hayashi, 1978. Instability of a gaseous envelope surrounding a planetary core and formation of giant planets. *Prog. Theor. Phys.*

60, 699-710.

Nakagawa, Y., C. Hayashi, and K. Nakazawa 1983. Accumulation of planetesimals in the solar nebula. *Icarus* **54**, 361-376.

Nakazawa, K. and S. Ida 1988. Hill's approximation in the three-body problem. *Prog. Theor. Phys. Suppl.* **96**, 167-174.

Nakazawa, K., S. Ida, and Y. Nakagawa 1989. Collisional probability of planetesimals revolving in the solar gravitational field I. Basic formulation. *Astron. Astrophys.* **220**, 293-300.

Ohtsuki, K., Y. Nakagawa, and K. Nakazawa 1988. Growth of the Earth in nebula gas. *Icarus* **75**, 552-565.

Ohtsuki, K and S. Ida 1990. Runaway planetary growth with collision rate in the solar gravitational field. *Icarus* **85**, 499-511.

Ohtsuki, K., S. Ida, Y. Nakagawa, and K. Nakazawa, 1993. Planetary accretion in the solar gravitational field. In *Protostars and planets III*, (E. H. Levy and J. I. Lunine, Eds.), pp.1089-1107. Univ. of Arizona Press, Tucson.

Safronov, V. S. 1969. *Evolution of the Protoplanetary Cloud and Formation of the Earth and the Planets*, NASA Tech. Trans. F-677. Nauka, Moscow.

Stewart, G. R. and G. W. Wetherill 1988. Evolution of planetesimal velocities. *Icarus* **74**, 542-553.

Wetherill, G. W. 1980. Formation of the terrestrial planets. *Annu. Rev. Astron. Astrophys.* **18**, 77-113.

Wetherill, G. W. and G. R. Stewart 1989. Accumulation of a swarm of small planetesimals. *Icarus* **77**, 330-357.

Wetherill, G. W. and G. R. Stewart 1993. Formation of planetary embryos: Effects of fragmentation, low relative velocity, and independent variation of eccentricity and inclination. *Icarus* **106**, 190-209.